GEORG-AUGUST-UNIVERSITÄT GÖTTINGEN

GEOMAR

Master's Thesis

Frischwasservariabilität im subpolaren Wirbel des Nordatlantiks von 1993 bis 2016 anhand von ECCO-Reanalysedaten

Freshwater variability in the North Atlantic subpolar gyre from 1993 to 2016 based on ECCO reanalysis data

prepared by

Anna-Marie Strehl

from Berlin

at the GEOMAR-Helmholtz Centre for Ocean Research Kiel

Thesis period: January 6, 2019 until February 28, 2020

First referee: Dr. Marilena Oltmanns

Second referee: Prof. Dr. Jörg Enderlein

Abstract

This thesis contributes to the investigation of the freshwater (re-)distribution in the North Atlantic in the decades around the turn of the millenium (1993-2016). The examinations are based on ECCO reanalysis data [1–3], which is used to describe the freshwater variability in the subpolar gyre (SPG). Possible driving mechanisms for variability and exchange with the surrounding regions are discussed.
The freshwater variability in the subpolar gyre of the North Atlantic can be divided into three periods in the investigated time intervall (1993-2016). The first period (until 2000) shows high variability and an overall salinity increase. During the 2000s, the freshwater content stagnates. Since about 2009, the salinity decreases, while again an intensified variability is found. This is peaked by an extreme freshening event in 2011. Over the total period from 1993 to 2016, the whole subpolar North Atlantic is freshening. The deep layers (below 200 m) seem to be isolated from the freshwater variability in the upper ocean layers.
Diffusive and turbulent freshwater fluxes are found to be the main driver of mixed layer variability, while advective transports determine the freshwater content in the deep layers of the SPG. Impacts of the total freshwater surface fluxes are found in the western SPG, whereas precipitation has a negligible contribution. The surface freshwater entries are transported via the Labrador Current and the East Greenland Current and enter the SPG at the Canadian coast. The transport inside the gyre is mainly from the Canadian coast in northeast direction.

Zusammenfassung

Diese Arbeit trägt zur Untersuchung der Frischwasser (Um-)Verteilung im Nord Atlantik in den zwei Dekaden um die Jahrtausenwende (1993-2016) bei. Die Frischwasservariabilität im subpolaren Wirbel (SPG) wird anhand von ECCO-Reanalysedaten [1–3] beschrieben. Mögliche Mechanismen, die die Variabilität beeinflussen, sowie der Austausch mit den umgebenden Regionen werden diskutiert.
Die Frischwasservariabilität im subpolaren Wirbel des Nord Atlantiks kann in drei Phasen innerhalb der untersuchten Zeitspanne (1993-2016) unterteilt werden. Die erste Phase (bis 2000) ist von hoher Variabilität geprägt. Insgesamt zeigt diese Phase eine Zunahme des Salzgehalts. Während der frühen 2000er stagniert der Frischwassergehalt. Etwa 2009 beginnend nimmt der Salzgehalt in der dritten Phase ab, während erneut erhöhte Variabilität verzeichnet werden kann. 2011 kommt es zu einem Ereignis besonders hohen Frischwassergehalts. Insgesamt wurde über die gesamte untersuchte Zeitspanne eine Frischwasserzunahme im subpolaren Nordatlantik festgestellt. Schichten unterhalb von 200 m zeigen sich isoliert von der Frischwasservariabilität in den darüber liegenden Schichten.
Als wichtigste Quelle für die Variabilität der oberen Schichten sind diffusiver Trans-

port und Turbulenz zu nennen. Salzadvektion und Volumentransport bestimmen den Frischwassergehalt in den tieferen Schichten des subpolaren Wirbels. Einfluss durch Oberflächenflüsse ist vor allem im westlichen subpolaren Wirbel zu finden, wobei Niederschläge einen zu vernachlässigbaren Beitrag stellen. Oberflächeneinträge in den subpolaren Nordatlantik werden entlang des Labradorstroms und des Ost-Grönlandstroms transportiert, wobei der Labradorstrom vor der kanadischen Küste in den subpolaren Wirbel eintritt und somit Frischwasser zuführt. Der Transport innerhalb des Wirbels erfolgt hauptsächlich von der kanadischen Küste in Richtung Nordosten.

Contents

1. Introduction

The ocean covers 71 % of the earth's surface [4]. Similar to the continents, the oceans's surface interacts with the atmosphere and therefore has a large influence on the atmospheric circulation [5]. Together, they build a system which determines the climate on earth [6]. There are lots of quantities, which are exchanged at the air-sea-interface, starting with freshwater (evaporation, rain)[6], gases like CO_2 or oxygen [7] and also abstract quantities such as energy (heat) [8] and momentum (wind stress) [9]. The ocean is often termed the flywheel of this climate system, because of its content of energy: a layer of about 3 m thickness of the ocean contains as much heat as the entire atmosphere [10]. Furthermore, it acts like a low pass filter in absorbing rapid atmospheric fluctuations and it transfers mechanical energy across space and time scales [10].

In times of changing climate, the ocean should get more and more attention, since it acts as a gigantic storage for all the quantities named above. The oceanographer's exercise is first to sketch the state of the ocean. This is done continously with a broad spectrum of methods. Typically, one combines different measuring methods like Conductivity-Temperature-Depth (CTD) rosettes and Acoustic Doppler Current Profilers (ADCP), which can be done on research vessels, with moored measurements and also autonomously moving "laboratories" like gliders and floats. Additionally, data from satellites can be used, which mainly contain information about surface properties. From time series of states, one can derive patterns and make assumptions on the oceans's response to changes. Further details about the reanalysis data used in the following will be given in chapter 3.

In this thesis, only a small part of the world's oceans is investigated: the subpolar North Atlantic. Due to its geographical proximity to the european continent, this region plays a key role in the european climate [e.g. 11–13]. The subpolar North Atlantic is especially influenced by the Gulf Stream and its extension, the North Atlantic Current (NAC), which mainly transports warm and saline water from the southwestern North Atlantic

to the northeastern part [e.g. 14, 15]. But also cold water from the Arctic Ocean is transported into this region [16, 17]. The different currents are interacting in a complex way, which is described in more detail in chapter 2. There, an overview about the surrounding system of the subpolar gyre will be given, which is important to understand its behaviour and driving forces.

The subpolar North Atlantic is the transition region between the North Atlantic and the Arctic. Hereby, the confluence of different warm and cold water masses causes large circulations. An oceanographic *water mass* is an identifiable body of water with certian physical (temperature, salinity) and chemical (isotopic ratios, concentration of gases) properties that are distinct from surrounding water. The properties usually allow conclusions about its formation history (age and origin) [18].
Global warming has already caused a decrease in the volume of ice at high latitudes [eg. 19–22]. Now, the question arises, whether this will lead to a redistribution of global water resources and what effects this could have. Changes in the composition and temperature of the seawater are expected especially in subpolar regions. Piecuch et al. [23] examined the heat content of the North Atlantic between 1992 and 2016 and found a temperature increase of the upper 700 m during the 1990s, which switched into a temperature decrease in winter 2004/2005. They evaluated the same data set on which the present thesis is based. This publication is the starting point for the question under investigation in the following: Can the temperature variability also be found in the freshwater content or do the two variables vary independently of each other? If they show an overall similar behaviour, this would be an indicator for water mass exchange. Here, also the question comes up, whether a driving force for freshwater variability can be identified. I will have a look at this in more detail in chapter 5.
In order to discuss the results, it is helpful to include the findings of other groups, who also analysed different data sets. A few results of earlier investigations are summarized in the following paragraphs.

Boyer et al. [24], who used reanalysis data provided by the National Center for Environmental Prediction/National Center for Atmospheric Research (NCEP/NCAR), found an increase of salinity in the total North Atlantic from 1955 to 2006, while at the same time the subpolar North Atlantic has been freshening. This behaviour is similar to the precipitation-evaporation curve in corresponding regions, wherefrom they concluded,

that the freshwater content is mainly driven by atmospheric influences. Freshening of the eastern subpolar gyre from the 1970s to 2000 has been shown by Josey and Marsh [25], as well. They state, that the freshening is mainly driven by precipitation, which is the main contribution to the precipitation-evaporation curve. The freshening of the subpolar North Atlantic has been affirmed by several studies in different regions with diverse methods [26–30].
In 2008, Wu and Wood [31] simulated freshening of the subpolar North Atlantic without invoking increased freshwater surface fluxes. They got to the conclusion, that the freshening could be the result of changes of deep convection in the Labrador Sea. This could trigger a perturbed ocean circulation which redistributes the freshwater between the Arctic and the subpolar North Atlantic. Hence, the observed freshening since the 1970s is not necessarily caused by freshwater surface fluxes.
Around 1990, Boyer et al. observe a change of the behaviour towards a strong decrease of subpolar freshwater, which is not explainable with the atmospheric curves. This finding corresponds to the work of Hátún et al. [32]: They report an increase of salinity in the eastern subpolar North Atlantic starting in 1997. The results are found in both, model simulations (Ocean General Circulation Model (OGCM)) and observations (NCEP/NCAR) reaching from 1948 to 2004.
The tipping point in 2004/2005 found in the heat content by Piecuch et al. fits to a more recent study by Dukhovskoy et al. [33] who evaluated in-situ data of Argo floats. They confirm an increase of salinity from 1993 to 2005 in all ocean basins of the subpolar North Atlantic. Afterwards (until 2016/2017), a salinity decline has been measured. This effect shows up in the upper layer (0 m – 50 m), as well as in deeper layers (50 m – 200 m and 50 m – 500 m). Another result of the study shows freshening signals propagating from the Labrador Sea towards the eastern subpolar North Atlantic. These signals occured between 2005 and 2016 in the upper several hundred meters of the water column. During the propagation, the signals are weakening, which leads to a decreased magnitude of freshening in the northern basins. However, a study of Holliday et al. [34] shows, that a strong freshening signal propagated along the Gulf Stream and the NAC towards the eastern subpolar North Atlantic during 2012-2016. This signal did not enter the SPG.

Summarizing these studies, they agree about decreasing salinity from the 1970s towards the 1990s [24, 25]. For the 1990s, an overall increasing salinity trend is found, but different groups name different points in time when the upturn begins [24, 32, 33]: Boyer et al.

state ongoing freshening of the subpolar North Atlantic until 2006, whereas Hátún et al. [32] observe salinisation in the eastern subpolar gyre since 1997. Dukhovskoy et al. [33] already report salinisation since 1993. From 2004/2005, Dukhovskoy et al. find freshening in all basins of the subpolar North Atlantic until $\sim$ 2017. Dukhovskoy et al. and Holliday et al. see propagation of freshening signals from the western to the eastern SPG or from the western subtropical towards the eastern subpolar North Atlantic, respectively, in the early 2010s.
From the analysis of the ECCO salinity data, I will find a freshwater content which behaves similarly to the heat content found by Piecuch et al. [23] and the salinity study by Dukhovskoy et al. [33]: increasing salinity until the mid 2000s and freshening afterwards. The freshening is strengthend by a freshwater event in 2011.

After identification of the freshening behaviour, the question about driving mechanisms arises. Fluid mechanical processes involved in the (re)distribution of salt can be described by advection, diffusion and turbulence. Usually, external forces such as Coriolis force are also considered therein. In addition, fluxes between different systems can occure (here, this is mainly between ocean and atmosphere).
Earlier studies regarding these mechanisms identified precipitation-evaporation [24] or precipitation [25], respectively. Wu and Wood [31] also suggest changes in deep convection as possible cause for redistribution of water masses and therefore freshening of the subpolar North Atlantic.
This is in contrast to the data set used here, from which it can be derived, that precipitation is not determining the freshwater variability between 1993 and 2015, while the influence of surface freshwater masses running off from the coasts are an important factor. In chapter 6, I will discuss the results which will be presented in chapter 5. The methods for analysing and interpreting the data are explained in chapter 4. This also contains the definition of oceanographic quantities and locations which are relevant in this context.

2. Theoretical Background: The (subpolar) North Atlantic

In this chapter, the North Atlantic is introduced as an oceanographic system. First, usefull concepts which are important to characterize the system are presented. Afterwards, the "properties" of the North Atlantic such as typical layers and circulation patterns are displayed. With this, it will be possible to identify variability and changes in the subpolar North Atlantic in chapters 5 and 6 and to discuss the influence of different driving mechanisms.

2.1. Thermohaline Circulation

The vertical arrangement of liquids is determined by their densities [35]. If processes form a more-dense layer at the surface, the column will be unstable. This leads to downwelling of the more-dense liquid and upwelling of the less-dense liquid [35]. In the oceans, this vertical displacement is called *overturn* [4]. Stable water columns show an increasing density with increasing depths, while columns with a constant density over depth are neutral stable, which means that they can easily be mixed due to outer processes such as wind, waves and currents [4]. The water mass's density is determined by their salinity and temperature, where higher salinity and lower temperature lead to a higher density [35]. If temperature and salinity changes lead to an unstable density distribution, the resulting overturn is called *thermohaline circulation* [10]. In the ocean, the thermohaline circulation is the main cause for Meridional Overturning Circulation (MOC) which is defined as the zonal integral of the meridional and vertical circulation in all ocean basins [10]. Certainly, in the MOC also other effects like overturning due to Ekman transport (wind-driven transport) are included. In the Atlantic, this motion is called Atlantic Meridional Overturning Circulation (AMOC).

The distribution of variables in the ocean can be described by lines of constant values (so called *isolines*), which are perpendicular to the variable's gradient. The three most important types of isolines, which are used to characterize the ocean, belong to temperature (isobathytherms/isotherms), salinity (isohalines), and density (isopycnals) [36]. In the upper kilometer of the ocean, there are strong vertical gradients of oceanographic variables (especially of temperature and density) [35]. The zone with the maximal gradient is called *cline* and can be defined for all observable variables (thermocline, halocline, pycnocline, chemocline, ...). It marks the transition from surface layer to deep layer. The depth of the clines depends on surface forcings like for example incoming solar radiation (thermocline) and evaporation/precipitation patterns (halocline) [35].

In general, one can find at least two layers in the oceanic water column: the surface layer and the deep layer [4]. The surface layer is also called *mixed layer*, since it shows a homogeneous density distribution. During autumn and winter, cool surface temperatures are forcing an overturn and storms strenghten the mixing, so that a deeper mixed layer than in spring and summer is obtained [37]. A schematic view of the annual variability of water column layers can be seen in Fig. 2.1.

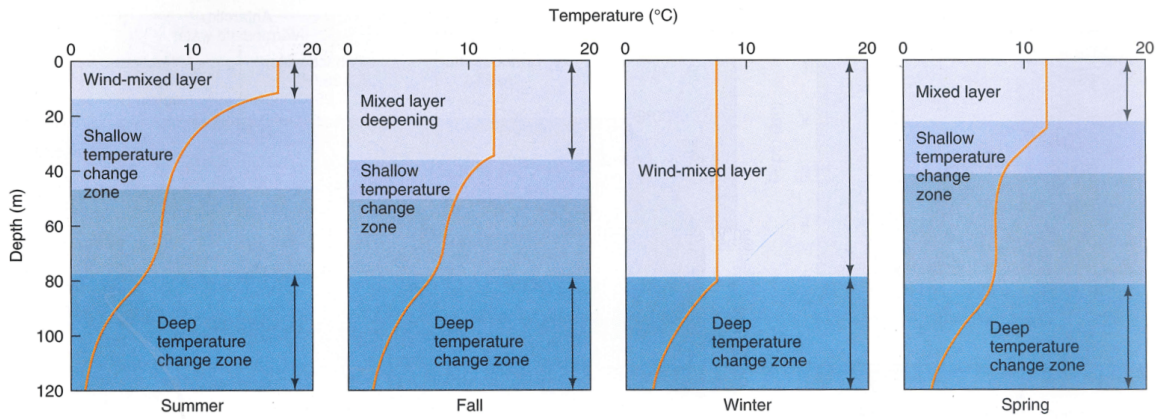

Figure 2.1.: Annual variability of mixed layer depths (schematic). The actual depths can vary on scales of 100 m. Adapted from [4].

To determine the actual mixed layer depth, several criterions are known. Kara et al. [37] are using a treshold for maximum annual temperature change, while Lorbacher et al. [38] apply the criterion of the shallowest extreme curvature of near surface layer density or

temperature profiles.
During most of the year, in the Atlantic Ocean the mixed layer is less than 150 m deep [38], which means that most of the exchange between ocean and atmopshere happens in this thin surface layer [36].

Gnanadesikan [41] developed a simple model of the overturning circulation and stratification: The stratification is represented by two homogeneous layers seperated by the pycnocline. Fig. 2.2(a) shows the mean density layers in the Atlantic. In the North Atlantic, the *Northern Sinking* and *Equatorial Upwelling* are used to model the flow balance, which emphasizes the strength of thermohaline circulation. The density distribution allows a distinction between different water masses with characteristic salinities and temperatures. Fig. 2.2(b) illustrates the temperature distribution, which can be separated in two layers along the pycnocline. Comparing this to Fig. 2.3, which shows the salinity distribution in the Atlantic, volumetrically large, deep water masses can be identified. In Fig. 2.3 also their meridional flow direction is indicated, which allows to recognize them as a part of the thermohaline circulation.

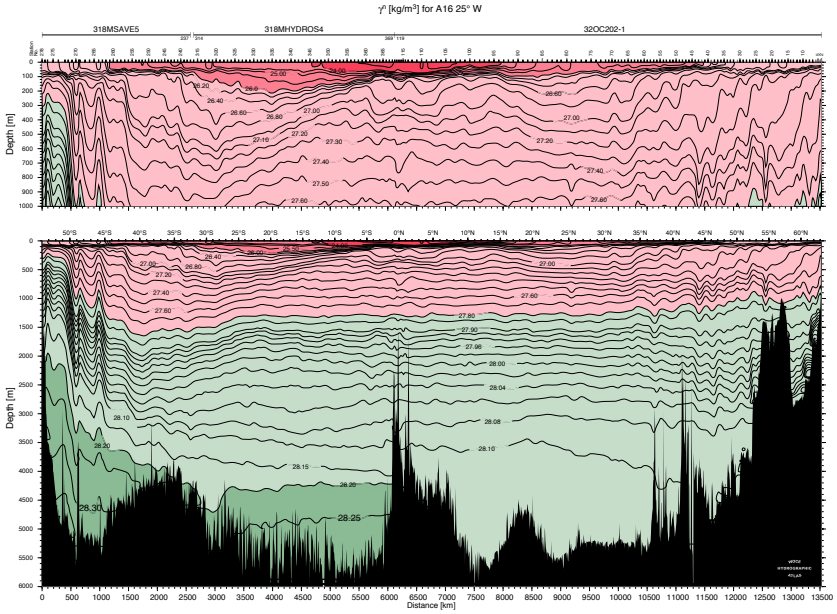

(a) Neutral density [$\mathrm{kg/m^3}$].

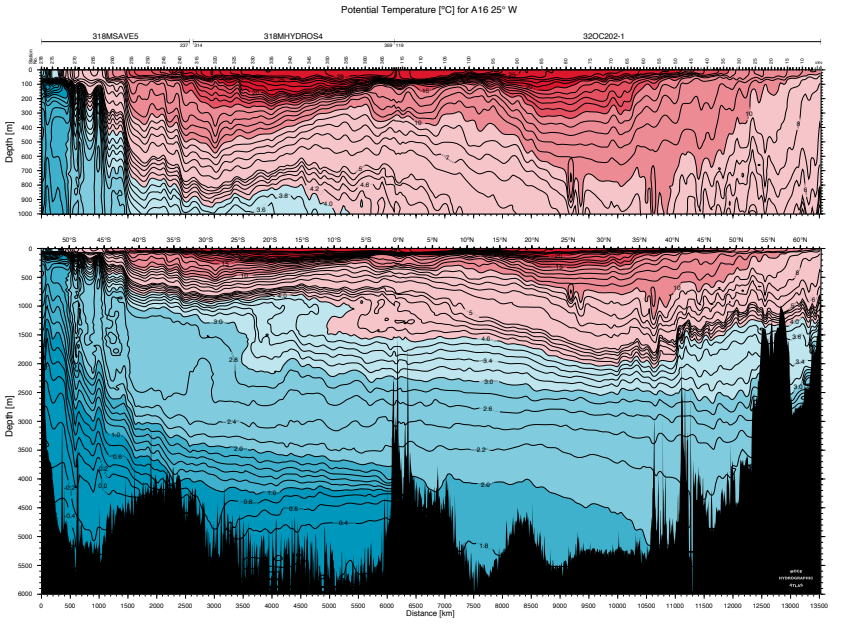

(b) Potential temperature [°C].

Figure 2.2.: Different quantities along the A16 section in the Atlantic at 25 °W from the WOCE-Atlas [39]. The colors show the seperation in two layers along the pycnocline. y-axis is depth [m], x-axis gives the latitude from 55 °N to 65 °S. The upper plot in each subfigure shows only the upper 1000 m of the water column, while the lower plot shows the full depth from 0 m to 6000 m, respectively.

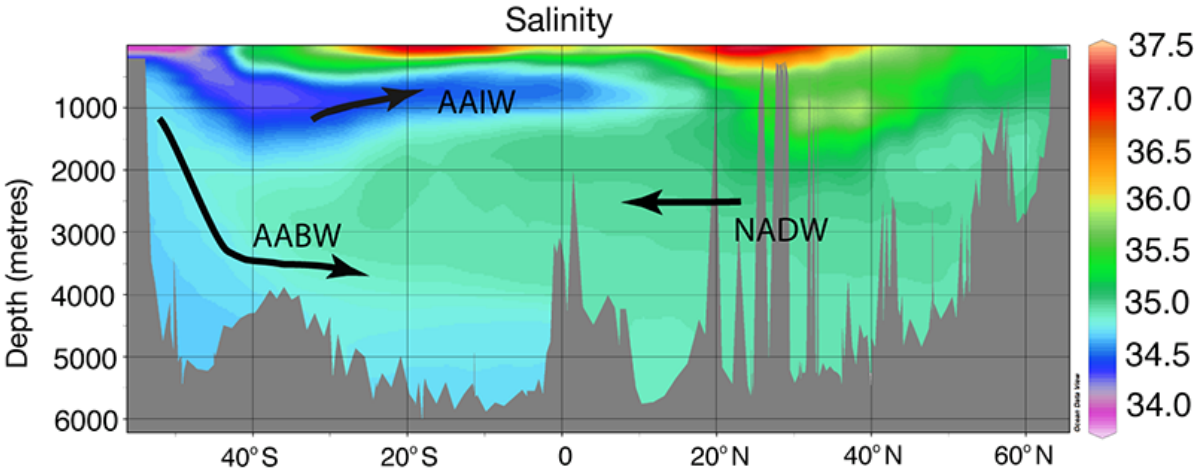

Figure 2.3.: Salinity [psu] in a section in the Atlantic Ocean. The arrows show the mean meridional direction of the major water masses: North Atlantic Deep Water (NADW), Antarctic Intermediate Water (AAIW), Antarctic Bottom Water (AABW). Adapted from [40].

2.2. North Atlantic current system

The main driver of the current system in the North Atlantic is the AMOC, which is both wind driven and buoancy driven [42]. The thermohaline circulation hereby represents the baroclinic component, while the Gulf Stream is an exmaple for a mostly barotropic current.
The subtropical North Atlantic is dominated by the subtropical gyre circulation. It mainly consists of warm and saline water and can be found at the surface layer [43, 44]. In the deep water, there is the southward flowing Deep Western Boundary Current (DWBC) with cold water from the northern seas [45]. The main currents of the North Atlantic circulation system are sketched in Fig. 2.4.

The Gulf Stream is the northern boundary current of the subtropical gyre [46]. The North Atlantic Current (NAC) is the northward extension of this surface current [10]. Together, they are carrying warm and saline water from the southwest towards the northeast. There, the NAC emits heat to the atmosphere and therefore cools which causes subsidence of the water masses [45]. The intermediate and deep waters flow along the Greenland tongue towards the Labrador Sea (East/West Greenland Current), where it becomes the southward flowing Deep Western Boundary Current (DWBC) [47, 48].

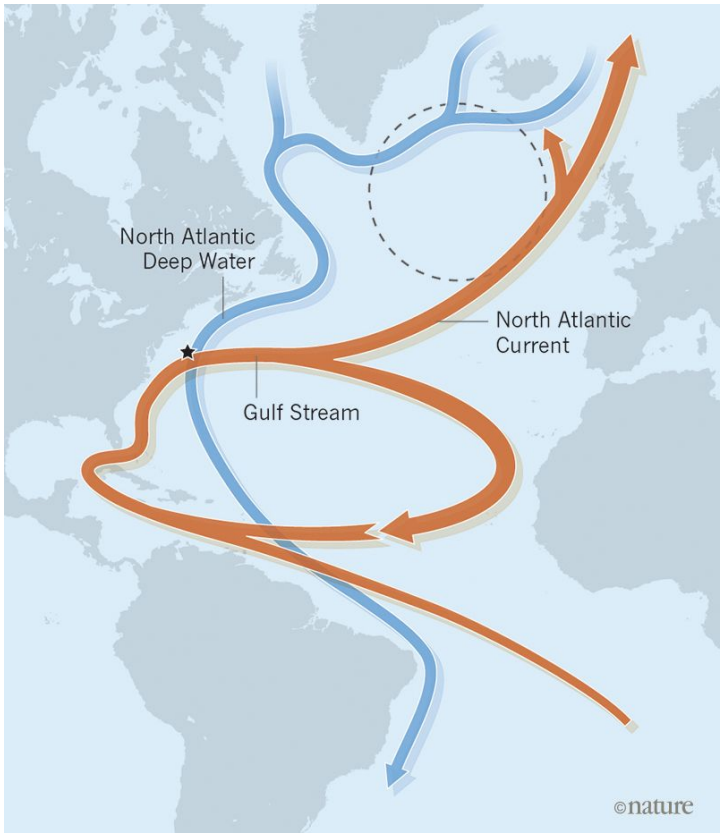

Figure 2.4.: AMOC: The AMOC is an ocean circulation system that consists of warm surface currents (orange) and cold deep-water return flows (blue), as shown in this simplified representation. The surface currents include the Gulf Stream, which feeds a branch of the AMOC known as the NAC. The deep-water return flows start from three branches that merge into the North Atlantic Deep Water (DWBC). The black star and the dashed line mark investigation zones of Thornalley et al. [49] and Caesar et al. [50]. Adapted from [51].

Subpolar North Atlantic

In the subpolar North Atlantic, the geometry of the basins and the mixing of water from the Atlantic with polar water masses lead to a more complicated current structure. As the subpolar North Atlantic will be investigated later on, it is important to get into more detail.

As already said above, the NAC transports warm and saline water from the subtropical North Atlantic to high latitudes, where it cools and therefore subsides. The actual

pathways of warm-to-cold conversion are more diverse than just sinking downwards. Chafik and Rossby [52] describe the process as follows:

> "One branch [of the NAC] continues into the Nordic Seas where very dense water is produced and eventually spills back into the deep North Atlantic, another branch weaves its way around the entire subpolar basin and the southern tip of Greenland to the Labrador Sea where intermediate water is formed, and the third branch is an overturning that takes place within the subpolar waters between Greenland and Scotland. Volumetrically, this is the largest branch, but in terms of heat loss, the Nordic Seas branch surrenders far more heat to the atmosphere than the other two combined. It thus plays the key role in maintaining a strong meridional overturning circulation."

The branching of the NAC can be seen in Fig. 2.5.
The East Greenland Current (EGC), coming from the polar region, merges with one branch of the NAC, the Irminger Current. At the Greenland tip, the current reflects northward and is now called West Greenland Current (WGC). In the Labrador Sea, parts of it merge with the Labrador Current and flow in southward direction [53]. The DWBC is following the same pathways in deeper layers [54]. At the Flemish Cape, the lower branch of the Labrador Current continues as DWBC along the east coast af the U.S., while the majority of the near-surface-waters from the Labrador Current reenters the NAC [55]. Fig. 2.5 gives an overview over the surface current system in the subpolar North Atlantic.

The NAC, Irminger Current, EGC/WGC and the Labrador current are the boundary currents of the subpolar gyre (SPG), which is located south of the tip of Greenland [55]. Since the currents are responsible for the volume transport in the subpolar North Atlantic, they also determine the advective bulk transport of observables like heat, salt and soluted gases. Therefore, they are an important component of the freshwater cycle in the ocean.

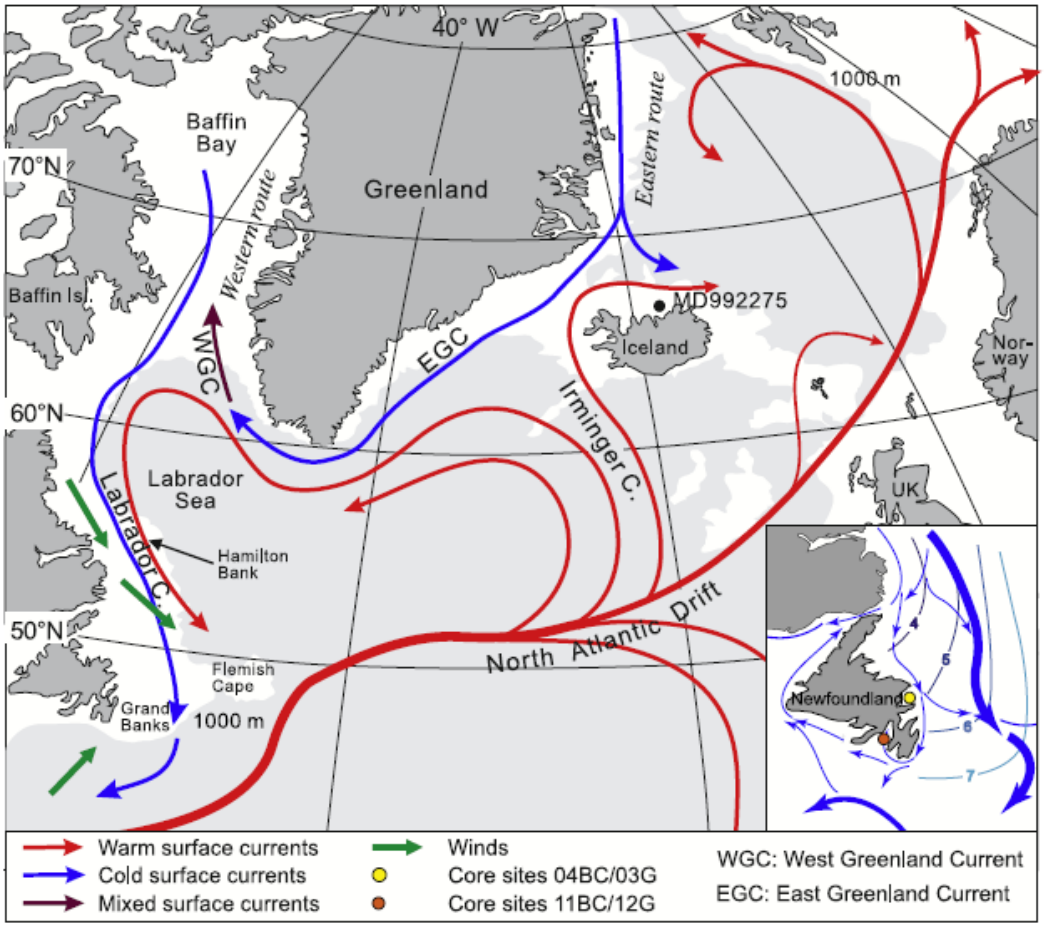

Figure 2.5.: Surface currents in the subpolar North Atlantic. Red/blue arrows indicate warm/cold surface currents, respectively; the prevailing wind directions are marked with green arrows. Adapted from [53].

3. Data

3.1. ECCO - Ocean data

In oceanography, three types of data are commonly used: in-situ data, reanalysis data and simulated data.
An advantage of in-situ data is, that it describes the actual state of the system. However, there are only small regions and defined time periods covered by the data due to missing continously spaced observation systems for the global ocean. Also, the data points are not necessarily spatially gridded and can contain gaps in their time resolution. Simulated data behaves in the opposite way in all the points mentioned: it is well gridded spatially and temporally. But being based on mathematical descripitions of the real system, it is not capable of reflecting reality. A possible solution to get smooth data sets is called *reanalysis*. The term covers different methods of data interpolation. The one applied to get the data set used in this thesis, is to use data points from in-situ measurements as a boundary condition for a model simulation.

To investigate the freshwater variability in the subpolar gyre, reanalysis data from the consortium for Estimating the Circulation and Climate of the Ocean (ECCO) [1–3] will be used. All calculations in the following chapters are based on Version 4, Release 3, which was the latest version available in October 2019.

Model

The model applied to in-situ data is the General Circulation Model of the Massachusetts Institute of Technology (MITgcm), which has been developed originally by Marshall et al. [56]. For Version 4 Release 3 of ECCO analysis, the MITgcm version described in [57] and documentated in [58] is used.
The ECCO Version 4 Release 3 files were produced using the “checkpoint66g” versions

of the MITgcm [59]. The corresponding software can be found at `http://mitgcm.org/download/other_checkpoints/` and `http://mit.ecco-group.org/opendap/ecco_for_las/version_4/checkpoints/contents.html`.

As underlying physical concept, an incompressible Navier-Stokes equation on a sphere with Neumann boundary condition has been implemented. Regarding the geometry, the ocean's basins and islands have been taken into account. The model describes the three-dimensional distribution of currents, potential temperature (T), salinity (S), pressure and density. Therefore, also the laws of thermodynamic have been taken into account using thermodynamic potentials for T and S. Terms describing inertia, coriolis force, basin geometry and dissipation have been included as well [56].
Since the model is based on the non-hydrostatic Navier-Stokes equation, it can be applied to various hydrodynamic problems on different scales depending on the grid resolution.

Volume and salt conservation

To interprete the data correctly, a look on the definitions of the variables in the ECCO data set and how they fulfill the conservation equations is needed. All variables named in the equations are explained in tab. 3.1, all used variables from the ECCO data set are listed in tab. 3.2.

To reach conservation of volume, the total surface height anomalies $G^{\eta,\text{tot}}$ have to be balanced by vertical and horizontal convergence $G^{\eta,\text{conv}}$ and additional volume fluxes at the surface $G^{\eta,\text{force}}$. The single terms are defined as follows [60]:

$$\begin{aligned} G^{\eta,\text{tot}} &= G^{\eta,\text{conv}} + G^{\eta,\text{force}} \\ \Leftrightarrow \frac{1}{H}\frac{\partial \eta}{\partial t} &= -\nabla_{z^*}(s^*\mathbf{v}) - \frac{\partial w}{\partial z^*} + s^* F \end{aligned} \tag{3.1}$$

The horizontal convergence is covered by the variables UVELMASS and VVELMASS of the ECCO data set, the vertical convergence by WVELMASS, respectively. The surface fluxes are contained in oceFWflx, which will be used for the analysis of the freshwater fluxes in the analysis part of this thesis.

For the salt budget, a contribution of diffusive fluxes has been taken into account [60]:

$$\begin{aligned} G^{S,\text{tot}} &= G^{S,\text{adv}} + G^{S,\text{force}} + G^{S,\text{diff}} \\ \Leftrightarrow \frac{\partial(s^* S)}{\partial t} &= -\nabla_{z^*}(s^* S \mathbf{v}_{res}) - \frac{\partial(S w_{res})}{\partial z^*} + s^* F_S + s^* D_S \end{aligned} \tag{3.2}$$

The different advection terms can be found in the ADVx_SLT, ADVy_SLT and ADVr_SLT for horizontal and vertical advection, respectively. Corresponding terms for explicit and implicit diffusion can be found with the labeling DFxE_SLT etc. It is important to notice, that the forcing terms are not including surface freshwater fluxes. This is due to the distinction between salt and salinity: while salinity describes a concentration, salt is the amount of salt molecules. So, freshwater entries do not change the salt content, but the salinity. The forcing terms are including the total salt flux (SFLUX [$\mathrm{g/m^2\,s}$]) and the salt tendency due to salt plume flux (oceSPtnd [$\mathrm{g/m^2\,s}$]). The total salt tendency is given by the salinity SALT ([psu]) times the volume scaling factor s^* which is unitless and can be expressed in terms of ECCO variables as (1+ETAN/Depth).
The diffusion term D_S contains both diapycnal and isopycnal components, as well as turbulence in the mixed layer and convection [60]. The budget for salinity can be derived based on the conservation equations for salt and volume [60]. From the product rule, one gets:

$$\frac{\partial(s^* S)}{\partial t} = s^* \frac{\partial S}{\partial t} + S \frac{\partial s^*}{\partial t} \quad .$$

With the help of eq. (3.2), this can be solved for $\dfrac{\partial S}{\partial t}$, which is the salinity tendency.

$$\frac{\partial S}{\partial t} = -\frac{1}{s^*}\left[S\frac{\partial s^*}{\partial t} + \nabla_{z^*}(s^* S \mathbf{v}_{res}) + \frac{\partial(S\, w_{res})}{\partial z^*}\right] + F_S + D_S$$

Including, that $\frac{\partial s^*}{\partial t} = \frac{1}{H}\frac{\partial \eta}{\partial t}$, the volume conservation (3.1) can be placed in and the

following formulation holds [60]:

$$\begin{aligned} \frac{\partial S}{\partial t} &= \frac{1}{s^*}\left[S\,\nabla_{z^*}(s^*\mathbf{v}) - \frac{\partial w}{\partial z^*} - \nabla_{z^*}(s^* S\mathbf{v}_{res}) - \frac{\partial (S\,w_{res})}{\partial z^*}\right] && +F_S - S\,F + D_S \\ \Leftrightarrow G^{\dagger,\mathrm{tot}} &= G^{\dagger,\mathrm{adv}} && +G^{\dagger,\mathrm{force}} + G^{\dagger,\mathrm{diff}} \\ &= \frac{1}{s^*}\left[G^{S,\mathrm{adv}} - S\cdot G^{\eta,\mathrm{conv}}\right] && +G^{\dagger,\mathrm{force}} + G^{\dagger,\mathrm{diff}} \end{aligned} \tag{3.3}$$

Here, the forcing includes both salt fluxes as well as surface freshwater fluxes (converted to appropriate units through multiplication by salinity) [60].
From these terms, the salinity advection $G^{\dagger,\mathrm{adv}}$ is stated as advection of salt $G^{S,\mathrm{adv}}$ reduced by the volume transport convergence $G^{\eta,\mathrm{conv}}$:

$$G^{\dagger,\mathrm{adv}} = \frac{1}{s^*}\left[G^{S,\mathrm{adv}} - S\cdot G^{\eta,\mathrm{conv}}\right] \quad . \tag{3.4}$$

It is to notice, that the salinity advection (eq. (3.4)) consists of two contributions, which both have to be taken into account during the analysis.
All variables regarding the salinity are given in psu. For the present thesis, this has been converted to the SI unit $^{\mathrm{g}}/_{\mathrm{m}^3}$.

variable	explanation
$G^{\eta,\mathrm{tot}}$	total volume tendency
$G^{\eta,\mathrm{conv}}$	volume transport convergences
$G^{\eta,\mathrm{force}}$	sea surface forcing of volume distribution
$G^{S,\mathrm{tot}}$	total tendency of salt content
$G^{S,\mathrm{adv}}$	advective flux of salt
$G^{S,\mathrm{force}}$	redistribution of salt due to sea surface forcing (does not contain surface fluxes)
$G^{S,\mathrm{diff}}$	diffusive flux of salinity
$G^{\dagger,\mathrm{tot}}$	total salinity tendency
$G^{\dagger,\mathrm{adv}}$	advective flux of salinity
$G^{\dagger,\mathrm{force}}$	sea surface forcing of salinity distribution (contains surface forcing)

Table 3.1 – *Continued on next page*

Table 3.1 – *Continued from previous page*

variable	explanation
$G^{\dagger,\text{diff}}$	diffusive flux of salinity
η	surface height at air-sea or ice-sea interface
H	ocean depth
z	unscaled vertical coordinate
z^*	$= \frac{z-\eta(x,y,t)}{H(x,y)+\eta(x,y,t)}\, H(x,y)$, rescaled height coordinate $\in [-H, 0]$
∇_{z^*}	horizontal divergence in z^* frame
$\frac{\partial}{\partial z^*}$	vertical divergence in z^* frame
t	time
S	salinity
s^*	$= 1 + \frac{\eta}{H}$, scale factor
$\mathbf{v} = (u, v)$	resolved horizontal velocity
w	resolved vertical velocity
$\mathbf{v}_{res} = (u_{res}, v_{res})$	total horizontal velocity
w_{res}	total vertical velocity
	here, "total" means, that the Eulerian flow field as well as the bolus velocity are contained
F	volumetric freshwater flux forcing
F_S	surface forcing of salt
D_S	symbolizes parameterized diffusive mixing processes of salt

Table 3.1.: Explanation of variables used in this chapter after [60].

Model input

The ECCO group interpolates observed data to a global geodesic grid with a spacing of approximately 240 km [3]. The calculations contain „the entire three-dimensional volume of the ocean" [1]. The corresponding in-situ data has been measured by different scientific projects including several research cruises, field observatories, Argo floats [61],

Southern Elephant seals as Oceanographic Samplers (SEaOS) [62], several moorings, satellite measurements and the World Ocean Atlas [63]. The location of measurement is matched to the nearest point on the grid [3]. The exact data sources can be looked up in Fukumori et al. [3].

ECCO output

The results of the interpolation calculations are available at `https://ecco.jpl.nasa.gov/products/latest/` [64]. More information about the current version can be found at the same webpage.
The ECCO product provides 90 oceanographic variables in different temporal resolutions. For this work, only monthly means are used. They can be found in the directory `nctiles_monthly/`. The data contains data from January 1st 1992 to December 31st 2015 [3]. The used variables are described in tab. 3.2.

directory/variable	content/description	
SSH	Sea Surface Height Anomaly adjusted with global steric height change and sea-ice load	[m]
SALT	salinity	[psu]
UVELMASS	zonal mass-weighted component of velocity	$[\mathrm{m/s}]$
VVELMASS	meridional mass-weighted component of velocity	$[\mathrm{m/s}]$
ADVx_SLT	u component of advective flux of salinity at the western face	$[\mathrm{psu\,m^3/s}]$
ADVy_SLT	v component of advective flux of salinity at the southern face	$[\mathrm{psu\,m^3/s}]$
DFxE_SLT	u component of explicit diffusive flux of salinity at the western face	$[\mathrm{psu\,m^3/s}]$
DFyE_SLT	v component of explicit diffusive flux of salinity at the southern face	$[\mathrm{psu\,m^3/s}]$
oceFWflx	net surface freshwater flux into the ocean	$[\mathrm{kg/m^2\,s}]$
EXFpreci	precipitation	$[\mathrm{m/s}]$
EXFevapo	evaporation	$[\mathrm{m/s}]$

Table 3.2.: Description of used variables. All variables are given at each gridpoint as a monthly mean.

Due to the fact that there is no simple, robust and general way to re-arrange global model

output in a single two-dimensional map [appendix C in 2], the global grid is split into 13 tiles of 90x90 grid points each for the interpolation calculation. Their allocation can be seen in Fig. 3.1. For the North Atlantic region, tiles 3 and 11 are concatenated. This requires correct orientation of the velocity vector components. In Fig. 3.2, an example for successful concatenation can be seen.

The mean distance between two gridpoints is $\sim 0.6°$. There exist 50 layers of gridpoints for several ocean depths, which are non-equally spaced with a height difference between 10 m close to the ocean's surface and 456.5 m in deep water (spacing shown in Fig. 3.3). Each of these 90x90x50 grid points contains 288 values, which are the monthly means between 1992 and 2016.

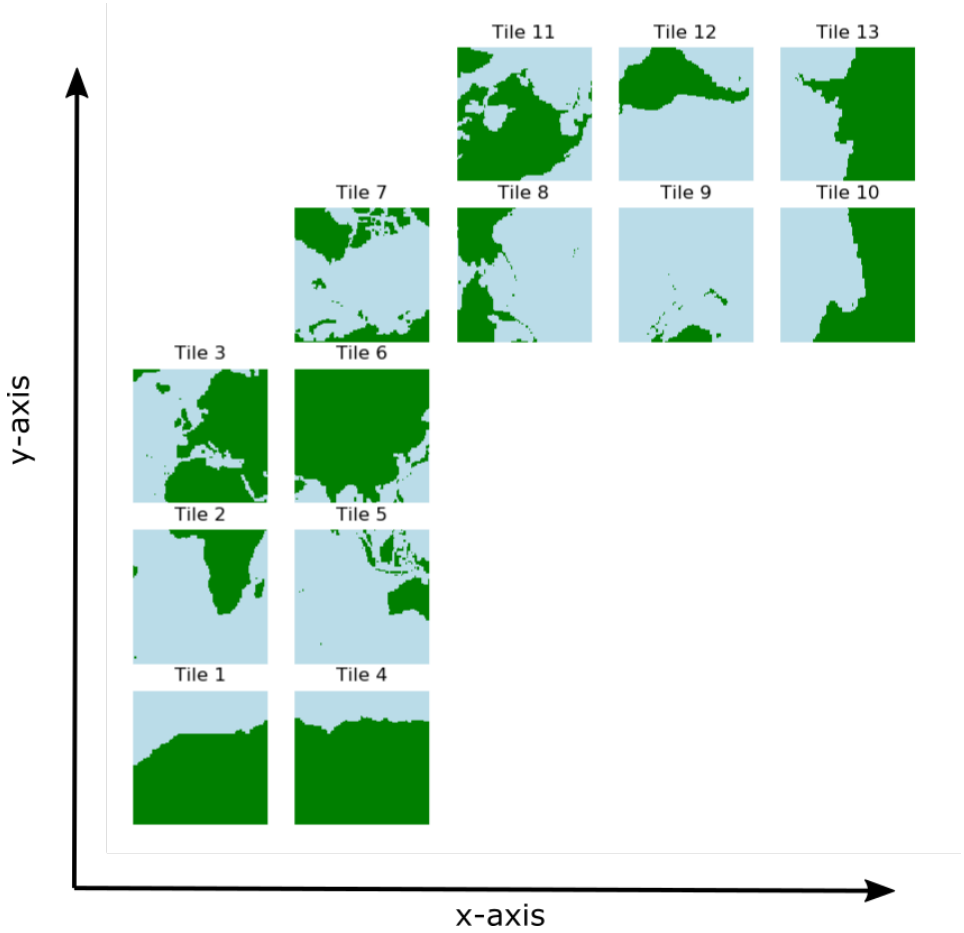

Figure 3.1.: Allocation and orientation of the grid tiles in the ECCO data set. The x- and y- direction for each tile used in the model are indicated with the axes. Adapted from [65].

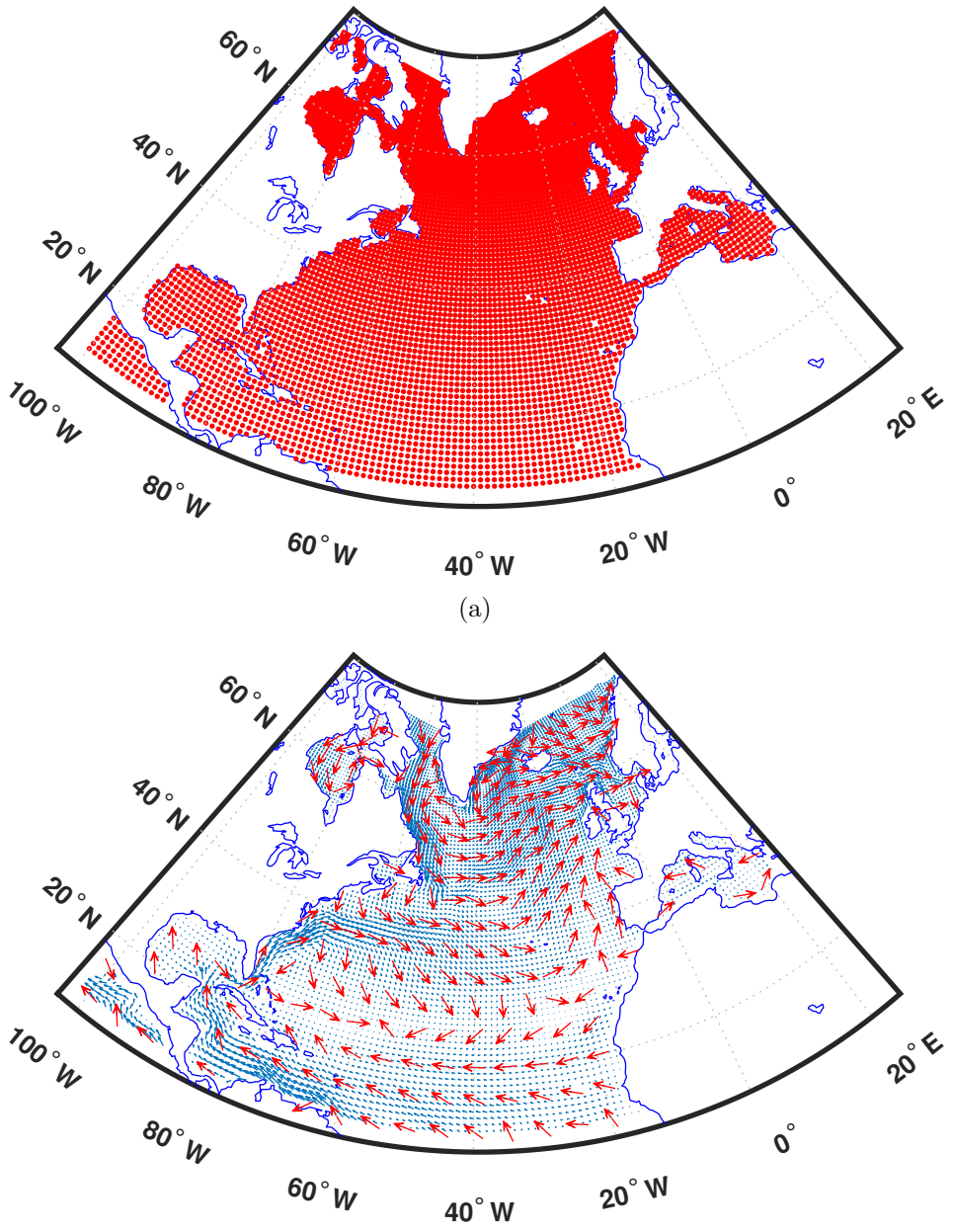

Figure 3.2.: Maps of the North Atlantic. (a) All grid points at the surface of the North Atlantic (red points). All variables (scalars and vectors) are available for all gridpoints. (b) Exemplary velocity vectors at the surface of the North Atlantic (red arrows). Darker blue background indicates higher absolute flow velocities.

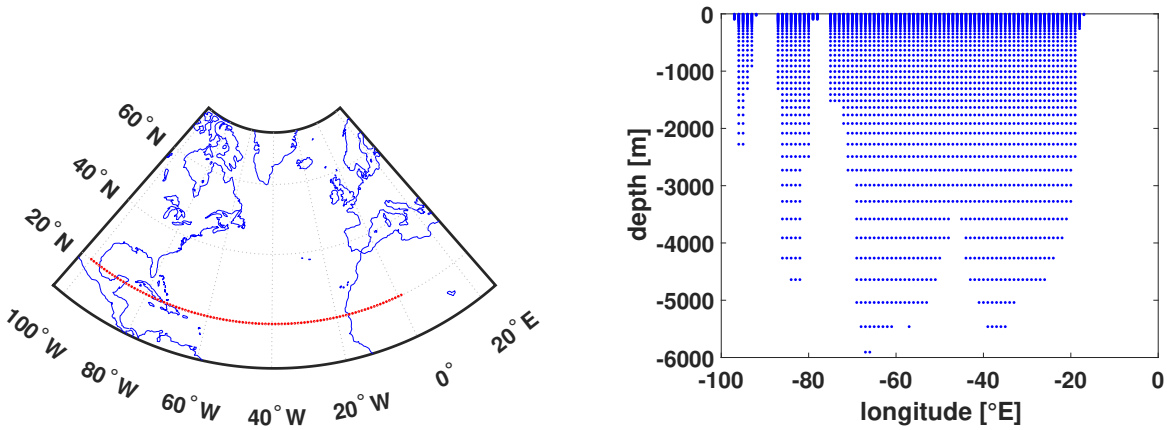

(a) Latitude of Cross Section.

(b) Depth profile of cross section shows layers of grid points. The white area indicates the bathymetry.

Figure 3.3.: Cross section at 20.1 °N.

4. Methods

4.1. Software

To evaluate the data, the programming language MATLAB, version R2016b [66] is used. To ensure an accurate unit transformation in the geographic coordinate system, the Gibbs-SeaWater (GSW) Oceanographic Toolbox [67] has, for example, been used to convert the salinity from psu into $^{g}/_{kg}$ or to calculate distances on the earth's sphere accurately.

4.2. Estimators for oceanographic data analysis

4.2.1. Trend analysis

Often, the data is influenced by the method of measurement (systematic errors) or shows variability on different scales. Depending on the aim of the analysis, the data has to be filtered to get rid of such effects. A first step is usually to find the overlaying trends.

Systematic Errors are usually characterized by an offset which can be found in all data points. Also non-linear influences from the measurement are possible. Such effects are non-physical and therefore have to be removed for a correct analysis.

Trends in the system itself can have any mathematical shape. Usually, systems are assumed to behave linearly on short time scales. An example from oceanography is the rise of sea level, which is assumed to be linear to calculate trends on scales of about 10 years [68]. To distinguish between trends which are caused by the measurement and trends caused by the system itself, one needs large data sets. If one can find different trends on different (time) scales, this is a hint for a behaviour of the real system and not of the measurement method. If a physical description of the system is already known, the

equation can be applied to the system to find suitable parameters. With trend analysis, three things are achieved:

1. The system can be described simplified with the general trend.
2. The general trend can be removed to find variability on other scales.
3. If available, it is tested, whether the physical description holds for this data set.

It should be mentioned, that trends do not have to be linear, but can also have polynomial shapes or follow other functions like the exponential or a sine-curve. The method to find trends which is used in the following is the "least-mean-square fit".

Removing seasonal trends

In oceanographic data, often seasonal trends can be found. To get rid of this influence, these trends are removed before analyzing the variability of the data. Therefore, the monthly mean over the total time period is subtracted from each monthly value.

Usage of winter data

Since the ocean has a high water capacity and therefore reacts slowly on outer influences, oceanographic analyses are usually using monthly to annual data. In the following, the interannual behaviour shall be sketched. To eliminate the influence of annual variability, only winter data is used, which represents the general behaviour in the North Atlantic well. Here, "winter" is defined as the mean over December, January and February (DJF).

4.2.2. Moving average

To smooth the data, a so called "window scan" or "moving average" is used. This means, that the value on each position or timestep becomes the mean of the surrounding values. The scale for spatial mean is set to two gridpoints in each direction. To calculate the temporal window-mean, two winters in past and future each are used.

4.2.3. Correlations

Sometimes, it is interesting to look at the connection between two variables. This can be quantified with calculating their correlation.

For two (random) variables X and Y, I define the correlation ρ as done by Shevlyakov and Oja [69]:

$$\rho = \rho(X,Y) = \frac{\mathrm{cov}(X,Y)}{\sqrt{\mathrm{var}(X)\mathrm{var}(Y)}} = \frac{\sum_{i=1}^{n}(x_i - \bar{x})(y_i - \bar{y})}{\sqrt{\sum_{i=1}^{n}(x_i - \bar{x})^2 \sum_{i=1}^{n}(y_i - \bar{y})^2}}$$

Here, x_i and y_i are observations from the sample with mean $\bar{x}$ and $\bar{y}$, respectively. To measure the statistical significance of the correlation, the p-value is used. This is the probability to obtain the found correlation coefficient from a random sample [70]. To be significant, a p-value smaller than 0.05 has to be reached. This characterizes the 95 %-significance level, which means that the probability to find this correlation value by chance is only 5 %. This treshold is commonly used in literature [70, 71].

4.2.4. Decomposition of data

For spatial data, it is interesting to know the system-internal coordinate system. Therefore, a so-called "Principal Component Analysis (PCA)" is helpful. The new coordinate system is spanned by orthogonal eigenvectors of the data's covariance matrix [72]. To sort them by importance, one calculates the explained variance, which quantifies how well the sample can be described by this vector. The corresponding eigenvalues are called *principal components*. A visualization of the eigenvectors for a gaussian data set can be seen in Fig. 4.1. For calculations, the `pca`-function of MATLAB [66] is used.
In oceanography, usually the term "Empirical Orthogonal Functions (EOFs)" is used instead of PCA, which is basically the same method [73]. The EOFs are the eigenvectors which span the system-internal coordinate system. In literature, one can find a slight difference in the use of both words [73]:

PCA method is used to perform the analysis on two or more variables that each evolve with time. One wishes to rearrange the data into "modes" that evolve in time following a specific function.

EOF method is used to perform the analysis on a variable that has a combination of spatial and temporal trends. Each spatial grid point is mathematically interpreted as single variable, which has a temporal evolution.

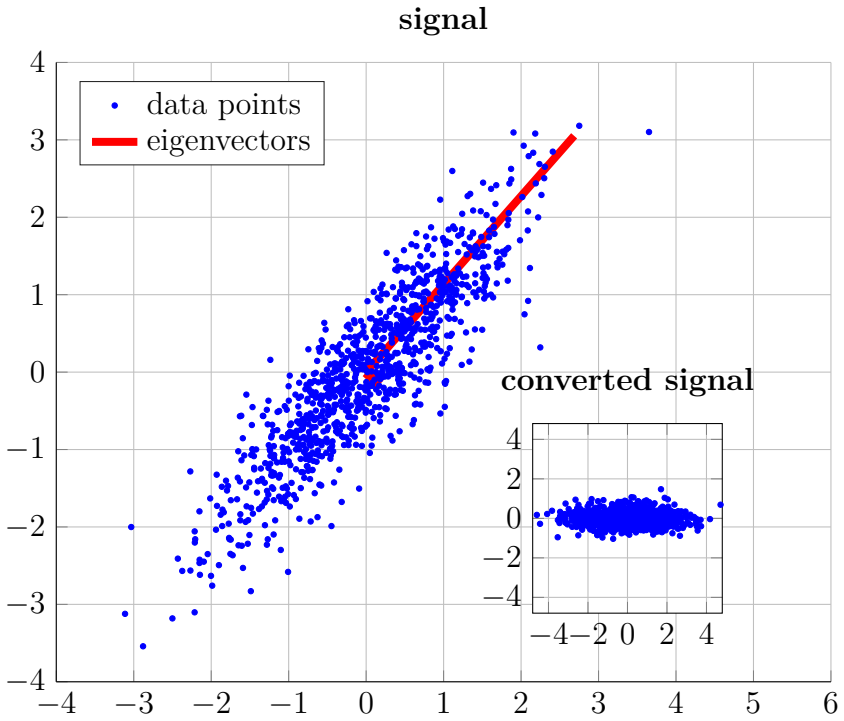

Figure 4.1.: Example for the result of the `pca` algorithm of MATLAB [66] for a 2-dimensional gaussian distributed signal. The inlet shows the signal in the coordinate system of eigenvalues.

This leads to the following description of the variable Z which depends on spatial coordinates $\mathbf{X}_i$ and/or time t in the new coordinates of eigenvectors ϕ_n [72]:

$$\begin{aligned} \text{EOF:} \quad Z(\mathbf{X}_i, t) \equiv Z_i(t) \quad &= \sum_{n=1}^{M} \alpha_n(t)\phi_n(\mathbf{X}_i) \\ \text{PCA:} \qquad\qquad\quad Z_i(t) \quad &= \sum_{n=1}^{M} \alpha_n(t)\phi_{ni} \end{aligned}$$

α_n is the Principal Component (PC) corresponding to the eigenfunction ϕ_n of the n^{th} mode. M is the order to which the EOFs/PCs are calculated. For the PCA method, i is the variable index, while in an EOF analysis i is the position index. This emphasizes, that finding EOFs is the same as performing a PCA with using the spatial coordinates as variables.

Summarizing, one uses the EOF-method to find groups of data points that vary together following a specified time function [73]. The principal components are used as indices, which quantify the strength of each mode.

4.3. Definitions

4.3.1. Freshwater

The salinity in the total North Atlantic spans from 14.8 psu to 40 psu which means that there is no real freshwater with salinity $S = 0$. Nevertheless, one can define how large the fresh water ratio in an oceanic volume is. Therefore, in the following, the unit $\frac{\mathrm{m^3\,freshwater}}{\mathrm{m^3\,seawater}}$, will be used. In this case, seawater is defined to have a reference salinity of $S_0 = 35.58\,\mathrm{g/kg} = 3.68 \times 10^4\,\mathrm{g/m^3}$. S_0 hereby corresponds to the mean salinity in the whole North Atlantic, averaged over all depths layers and all months between January 1992 and December 2015 in the ECCO data set.
The freshness f $[\mathrm{m^3/m^3}]$ of each point is then defined as

$$f = -\frac{S - S_0}{S_0} \quad .$$

For the freshwater content FW $[\mathrm{m^3}]$ it follows:

$$FW = \int_V f \,\mathrm{d}V \quad .$$

To illustrate the meaning of this definition, f is plotted for the North Atlantic in Fig. 4.2. Negative values correspond to water which has a salt concentration larger than S_0. Since the values of the freshwater content are strongly dependent on the size of the integrated region, for easier comparison, in the following everything will be calculated for the variable “freshness”.

Freshwater Fluxes

Freshwater fluxes will be used to describe the fresh water variability within the SPG. These can be divided into volume and surface flows. For the volume fluxes, the advective and diffusive salt transport will be used as an equivalent to describe the freshwater flow.

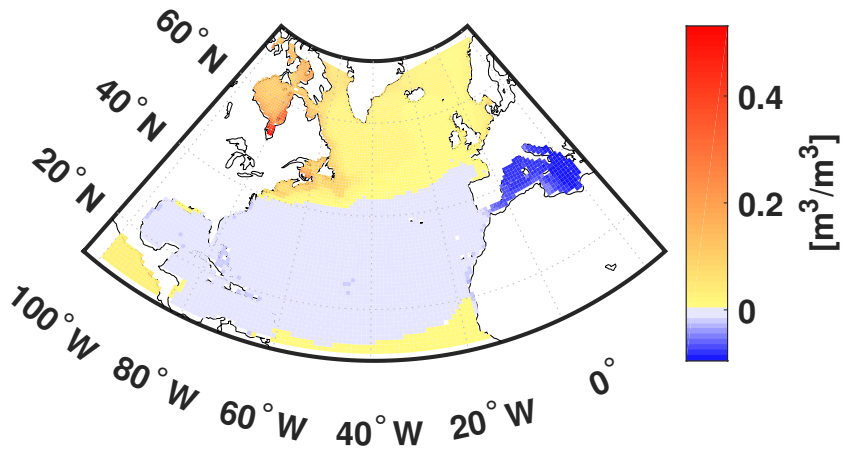

Figure 4.2.: Freshness of water in the North Atlantic. Averaged over the total basin depth and all available time steps (monthly values from January 1992 to December 2015).

Hereby, diffusion contains iso- and diapycnal mixing, as well as turbulence and convection [60]. The ECCO data set contains a file for the total freshwater surface fluxes. They are composed of precipitation, evaporation and river runoff. In the North Atlantic, river runoff also includes interaction with the cryosphere (melting and freezing of ice) [10]. To identify the major component of the surface fluxes, the single contributions will be analysed as well as the total surface fluxes. From the ECCO data set, no separate data concerning the river runoff exists. Therefore, only evaporation and precipitation will be compared to the total freshwater fluxes.

4.3.2. Subpolar gyre

The SPG is located at the southern tip of Greenland. It is built by its boundary currents, NAC, Irminger Current, EGC/WGC and Labrador Current [55]. To define the geographical boundaries, different methods are used, but all of them are based on SSH measurements.

An EOF analysis of the SSH variability gives the spatial pattern of variability while the PCs are used as *gyre index*. The gyre index can be interpreted in different ways, for example as a metric of the gyre's size [32] and strength [74].

In Fig. 4.3(b), the first EOF of SSH variability for the data set used in this thesis is shown. It is positive in the whole North Atlantic and explains only 2.3 % of the variance. This is much less than 10 % to 14 % found by different authors for similar time periods [75]. Possibly, this is due to different resolution of the used data points. Therefore, this

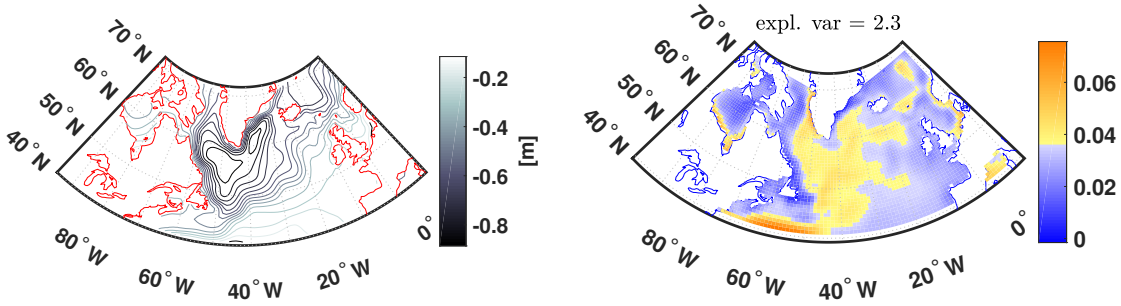

(a) Sea Surface Height (SSH)

(b) First EOF

Figure 4.3.: (a) Mean SSH averaged over all winters from 1992 to 2015 for each gridpoint in the subpolar North Atlantic. (b) First EOF of SSH in the same time period as (a). The explained variance of the SSH variability by this EOF is 2.3 %.

criterion is not applicable here.

For calculation of the gyre's area, Foukal and Lozier [75] also propose a different method: They define the subpolar gyre as the largest closed surface, which is enclosed by a constant SSH (cf. Fig. 4.3(a)). The interval chosen by Foukal and Lozier [75] to define the SSH to be constant is 1 cm. In the ECCO data set, this interval does not lead to any closed surface at all. Therefore, the interval has been set to 5 cm. Thus, for every time step, a closed surface could be found. The found regions now were shaped different than that found by Foukal and Lozier [75]. Especially in the eastern SPG, several northern boundaries showed a cut-off at 60 °N instead of the expected heart-shape. To get a second criterion, the SSH has been correlated with the gyre index found by Foukal and Lozier [75], since grid points in the subpolar gyre should show high correlation values with the gyre index. Only grid points with correlations on a significance level of at least 99 % have been accepted to be part of the SPG.

The intersection of points found with both methods has been calculated for all time steps. Intersecting points (i.e. points which fulfill both criteria) which show up in at least $^1/_5$ of all time steps finally have been defined as SPG. The interim results of finding the SPG and the final SPG points can be seen in Fig. 4.4.

Looking at the basin topography of the subpolar North Atlantic (Fig. 4.5), one can find a similar shape in the bathymetry. Below the subpolar gyre, there the water column is deeper than in surrounding regions. The Reykjanes Ridge acts as the topographic eastern boundary of the SPG, but protrudes into its hydrographic area. This also affects

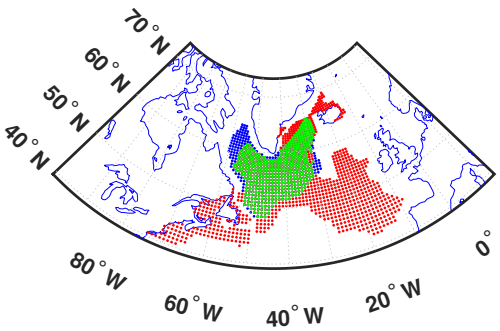

(a) Example for results of the different criteria for one (randomly chosen) time step: blue marks grid points which are only found with the 'closed surface' criterion, red marks grid points only found by the 'correlation' criterion and green marks points which fulfill both criteria.

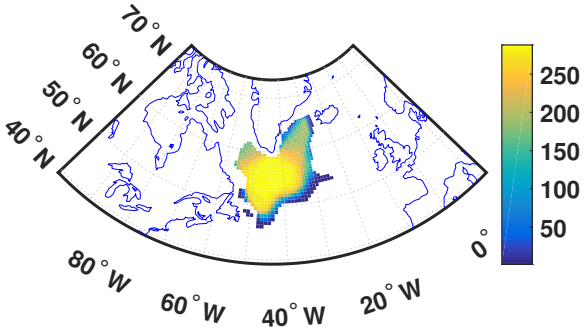

(b) Sum of all intersections from January 1992 to December 2015 (monthly values). Each occurence is counted as 1, so the colour indicates the number of occurence of each point in the intersection.

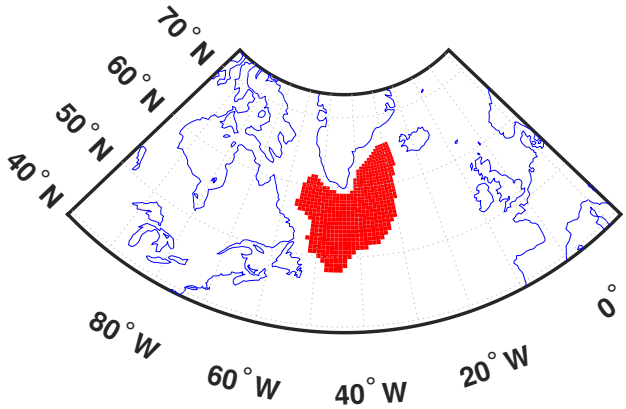

(c) All points which occure at least 1/5 of all time steps are defined as the SPG used for following analysis.

Figure 4.4.: Steps on the way to the definition of the SPG and final SPG points.

the flow direction in the deeper layers, as will be shown later (cf. Fig. 4.6).
The SPG is dynamically formed by boundary currents which follow mainly the basin topography [74, 76]. Due to this situation, one can find a homogeneous flow structure over the whole basin depth in the SPG area [76]. With this, it can be justified to investigate the SPG as a closed system, which interacts with the surrounding ocean by the boundary currents.

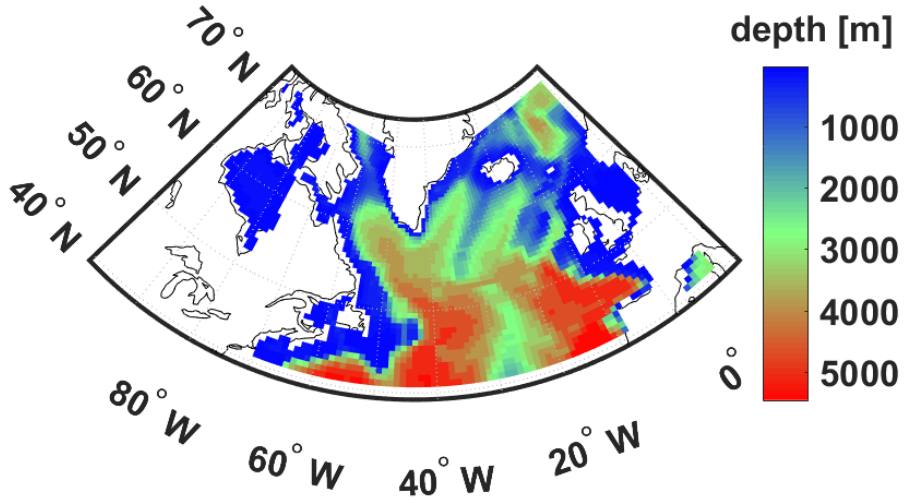

Figure 4.5.: Basin topography of the subpolar North Atlantic. The depths of each grid point is taken from the "land mask" given in the ECCO data set.

4.3.3. Subpolar gyre regions

To be able to differentiate the results, the SPG has been divided into different areas. Depending on the criterion for separation, one finds two possible segmentations, which are shown in the following.

The flow direction shows clear parts of more westward, southward or northeastward flowing regions (Fig. 4.6). This structure is preserved over the whole depth. Since the flow direction has a direct relation to transport, the found regions are used as regions of analysis in the following part. The regions have been defined and named as can be seen in Fig. 4.7(a).
In literature, another possible segmentation can be found [eg. 10, 29, 77, 78]: the separation then is made between eastern and western SPG (cf. Fig. 4.7(b)): These two regions are shown to behave unequally in salinity or temperature variability and respond differently to external forcings like the North Atlantic Oscillation (NAO).

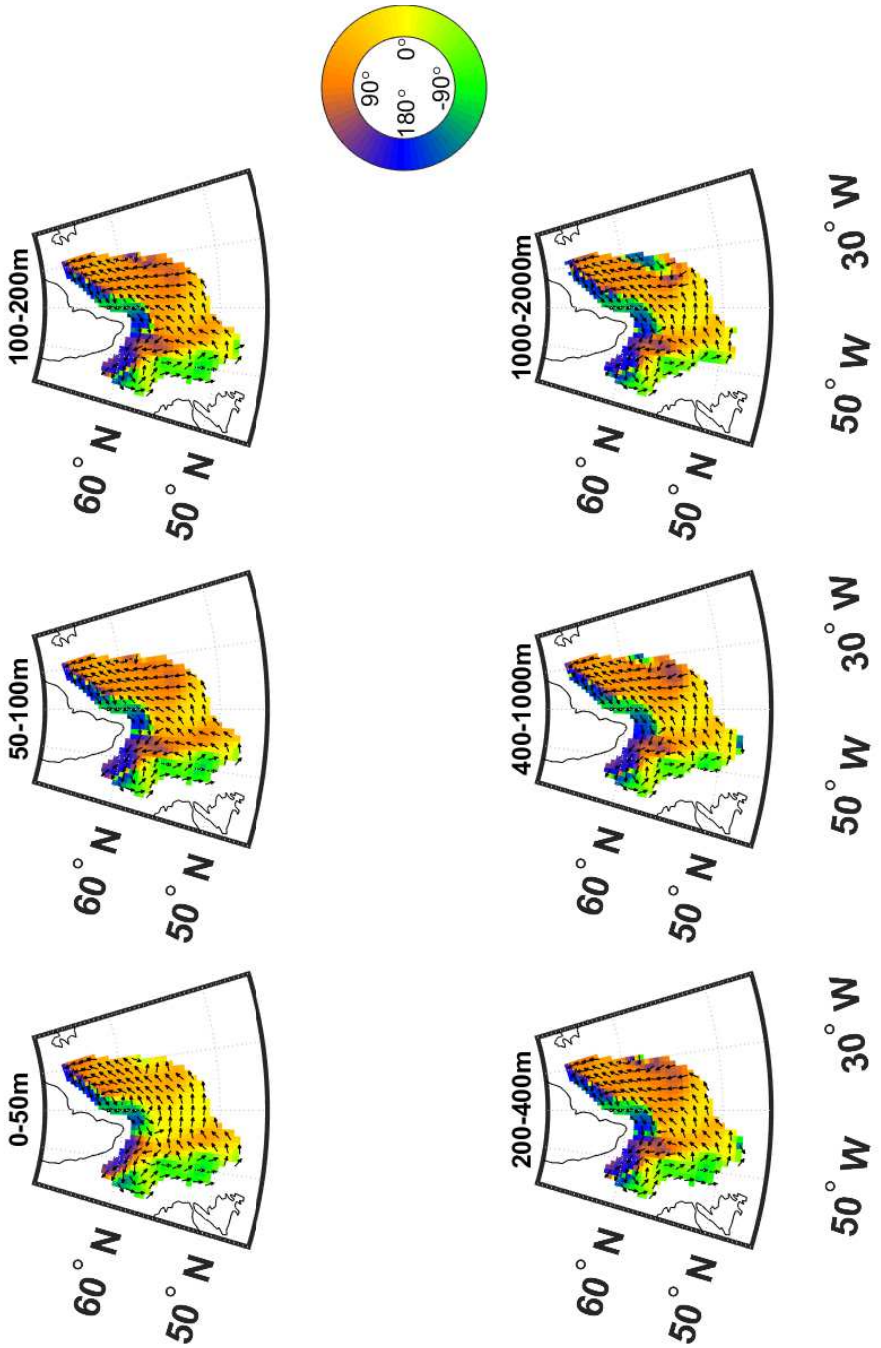

Figure 4.6.: Mean flow direction in different depth layers. 0° means flow towards east. Arrows are only a "guideline to the eyes" to simplify the translation from a colour to a direction. The mean is calculated over the indicated layer depths and over all winter months between 1992 and 2016. The direction is derived from the east- and northward volume flux velocity components of the ECCO data set.

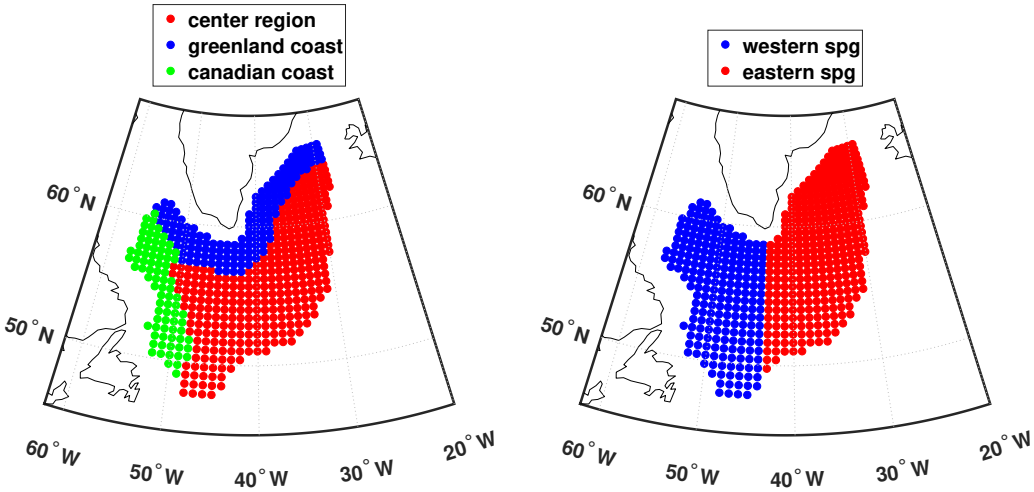

(a) Regions in the SPG defined by the mean flow directions.

(b) Regions in the SPG as can be found in literature.

Figure 4.7.: Different segmentations of the SPG.

5. Results

In the following, first the freshwater content and its variation will be described. Afterwards, different freshwater fluxes are correlated with the freshwater itself to see the strength of influence of the single fluxes. Therefore, a distinction between volume and surface fluxes will be made. For the volume fluxes, I am going to look at three terms (corresponding to eq. (3.3)): volume advection $G^{\eta,\mathrm{conv}}$, salt advection $G^{S,\mathrm{adv}}$ and salt diffusion $G^{S,\mathrm{diff}}$. Also the surface fluxes are composed of three contributions: precipitation P, evaporation E and river runoff R which includes also contributions from the cryosphere. To evaluate the importance of the single terms, first the total flux is analysed and compared to P and E later on.

5.1. Freshwater content in the subpolar gyre

Temporal Analysis

As one can see in Fig. 5.1, the freshness below 500 m depths is nearly constant over time in all six investigated regions. In general, there, the freshness is low compared to the upper layers. The variability in the top 200 m shows the same behaviour in all six regions, but different degrees of intensity. One observes more freshwater at the beginning and at the end of the investigated period, while in between, the salinity increases especially in the uppermost 100 m. In 2011, the freshening could be interpreted as a freshwater event, since this year can also be found to have an anomaly larger than two times the standard deviation. All years between 1995 and 1998 show high anomalies, so that in this time period no event can be singled out. For easier comparability to the following sections of analysis, the mean time series for the freshness in the mixed layer are shown in Fig. 5.2.

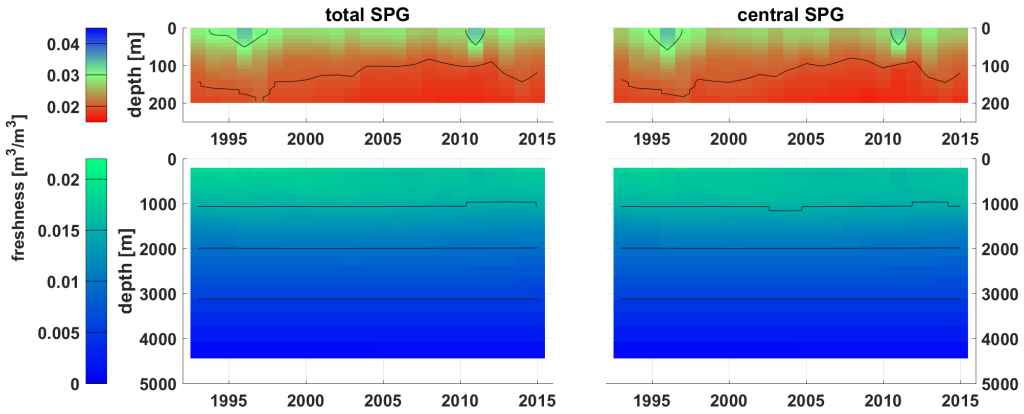

(a)

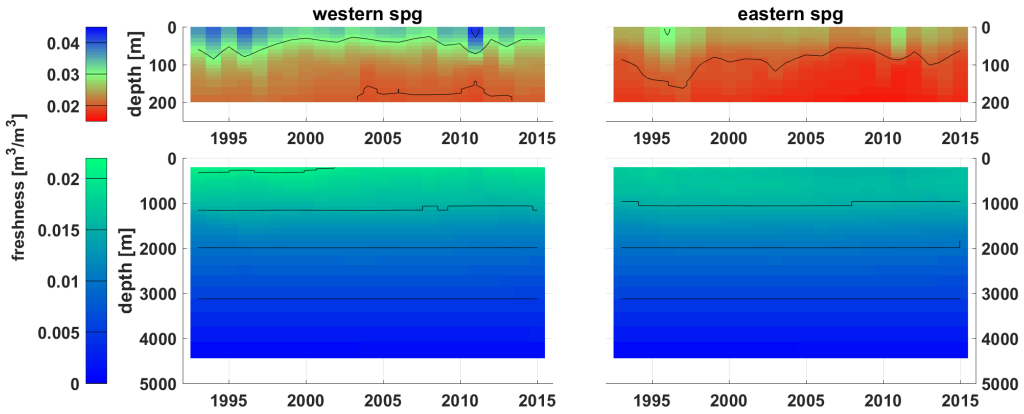

(b)

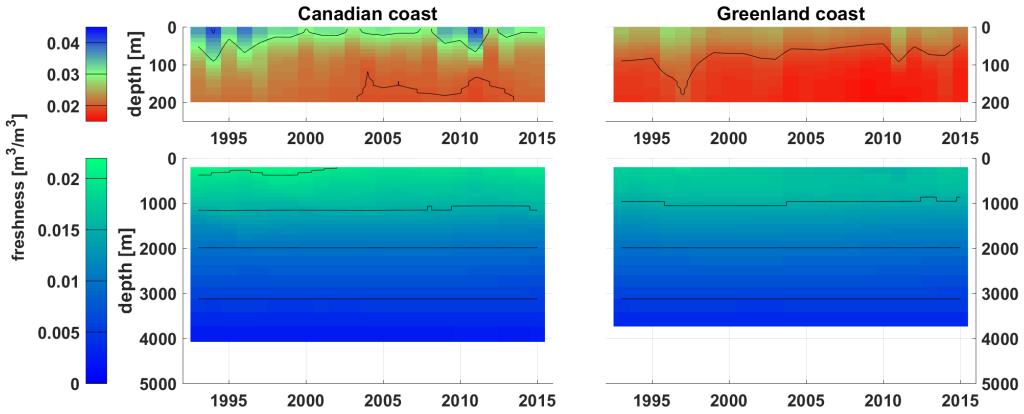

(c)

Figure 5.1.: Winter timeseries of freshness [m^3/m^3] as a function of depth. Each panel is averaged over the region specified in the supertitle. Upper panels show upper 200 m, lower panels show 200 m – 5000 m.

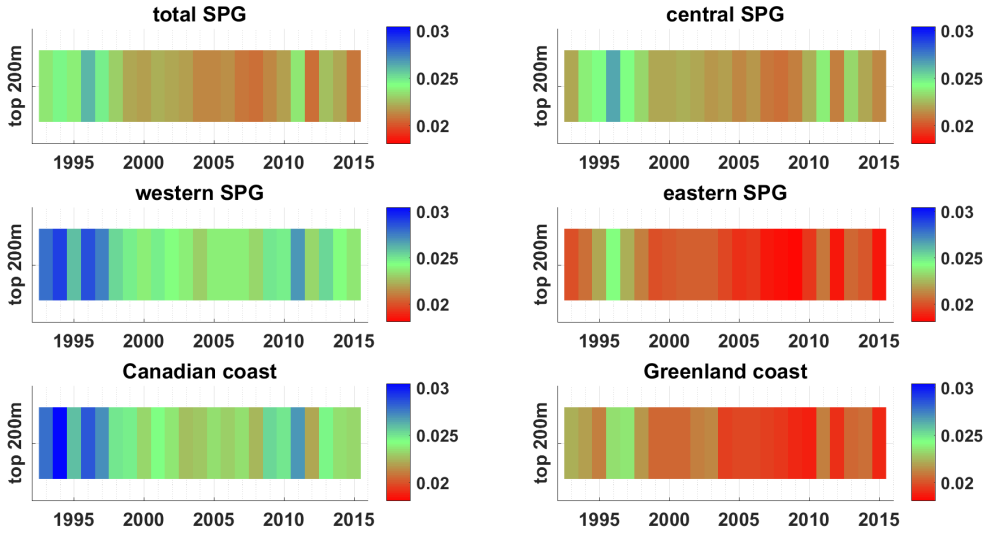

Figure 5.2.: Timeseries of mixed layer (top 200 m) freshness [m^3/m^3] during winter from 1993 to 2015 for specified regions. Averaged over mixed layer depth and specified area.

Comparing the different regions, one can see that the eastern SPG and the Greenland coastal region are very similar. The same holds for the western SPG and the Canadian coastal region. The separation in center region and boundary region (Fig. 5.1(b)) seems to be an average of both situations, but still shows the characteristic strong freshwater years. The intensity of the 2011 event of strong freshness is much lower in the eastern than in the western SPG.

Spatial Analysis

The different layers in Fig. 5.3 show an increase of salinity from top to bottom. The SPG has a homogeneously distributed freshness, which also holds for higher resolutions (Fig. 5.3(b)). The variability of freshwater in the SPG can be found on a range between 0 and 0.04 m^3/m^3, which is $\frac{1}{10}$ of the range in the total subpolar North Atlantic. Even on this intervall, only a slightly higher freshwater content at the western boundary and the southern tip of the SPG can be seen. This corresponds to the higher freshwater content of the western SPG in Fig. 5.1. Especially the freshwater boundary through the Labrador Sea along the western boundary of the SPG stands out: Probably the basin topography inhibits the exchange between the shallow and deep region.

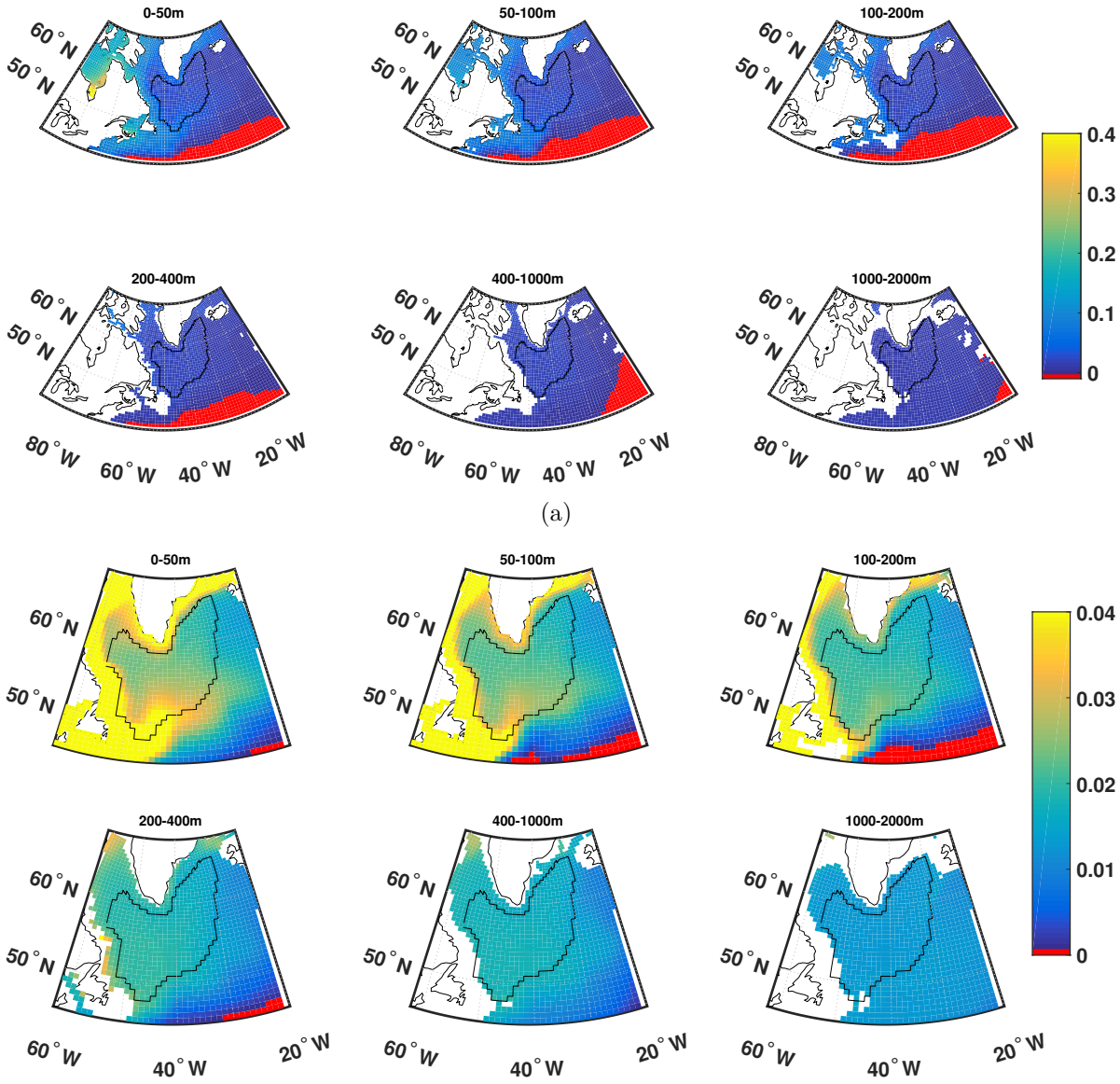

Figure 5.3.: Mean freshness [m^3/m^3] for each depth layer, averaged over all winters from 1993 to 2015. (a) Total subpolar North Atlantic (b) SPG only. Note the different color scales.

How can the temporal variability and the spatial homogeneity be explained? Which mechanisms cause this behaviour? To find solutions to these questions, in the following chapters, the freshwater fluxes and their correlations with the freshwater content are analysed.

Freshwater variability

Temporal Analysis

As the focus of this thesis is on freshwater variability, the changes of freshness are going to by analysed in the following paragraphs. Therefore, the difference between two consecutive years has been calculated. The corresponding time series are shown in Fig. 5.4.

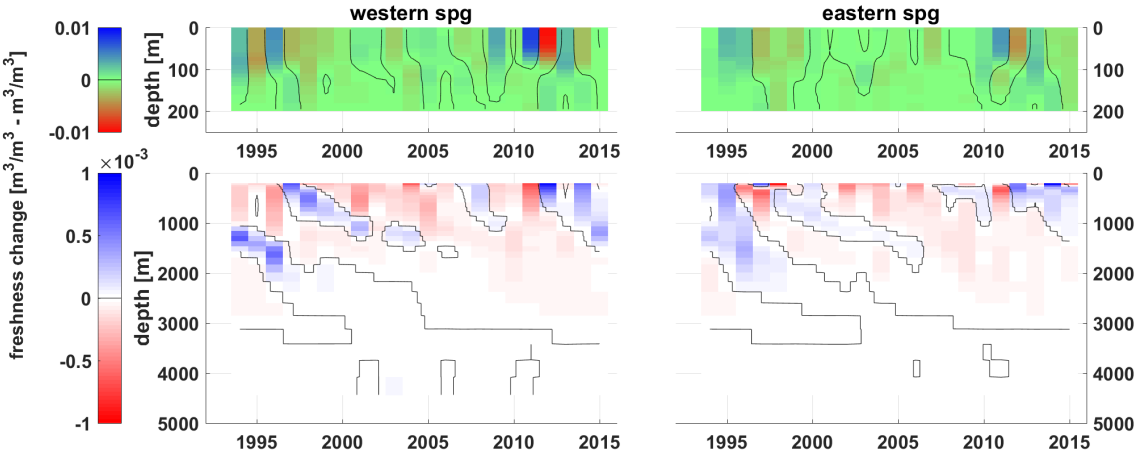

(a)

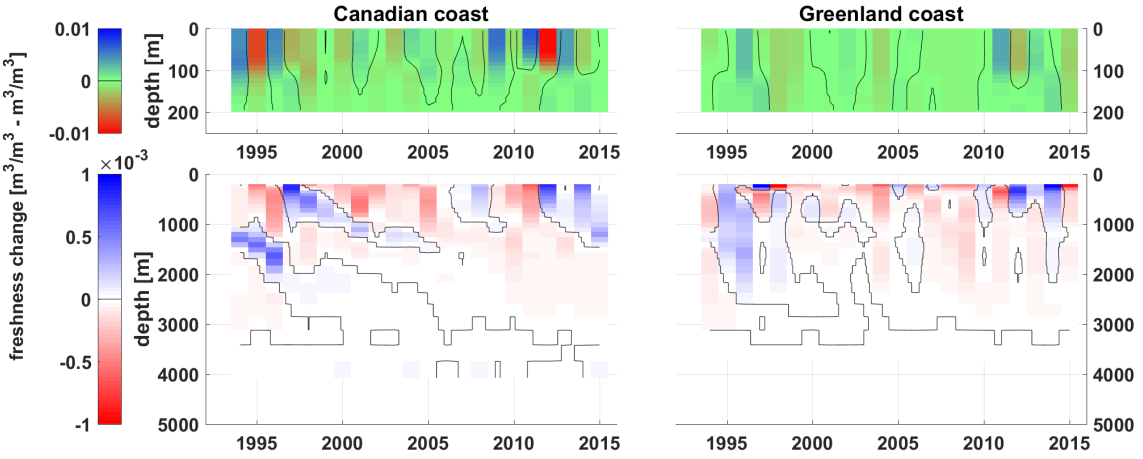

(b)

Figure 5.4.: Spatially averaged freshwater changes [$^{m^3}/_{m^3}$ - $^{m^3}/_{m^3}$] between successive winters for different regions as a function of depth and time.

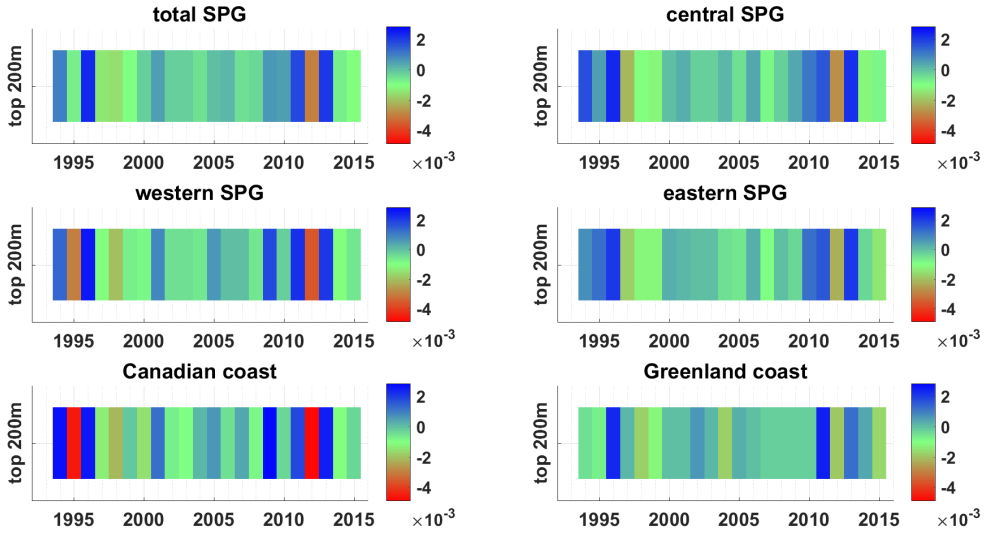

Figure 5.5.: Timeseries of mixed layer (top 200 m) freshwater changes between successive winters $[m^3/m^3 - m^3/m^3]$ from 1994 to 2015 for specified regions. Averaged over mixed layer depth and specified area.

Especially in the upper 200 m (see also Fig. 5.5), the results from Fig. 5.1 are supported. The western region/Canadian coastal region does not only show higher ratio of freshwater, but also stronger changes than the eastern region/Greenland coastal region. The extreme freshwater decrease from 2011 to 2012 emphasizes the strength of the increase in 2011. In general, the years 1993 – 1999 and 2009 – 2015 are found to show higher variability than the decade in between (cf. Fig. 5.5). The deep layers show variability on a scale which is smaller by one order of magnitude than the upper layers (Fig. 5.4). On this scale, anomalies which develop stair-like towards deeper layers are visible. They indicate subduction with a transport rate of approximately 200 m to 300 m depth per year.

Spatial Analysis

One has to be careful interpreting the temporal mean of freshwater changes (Fig. 5.6). A small average value can mean that there is low variability at all, or that there are positive and negative deviations canceling out each other. The average can also be understood as difference between the last and the first year in the investigated period. Here it is shown, because three clearly bounded regions with different properties can be identified in the upper 100 m. In deeper layers, the regions become more and more blurred and below

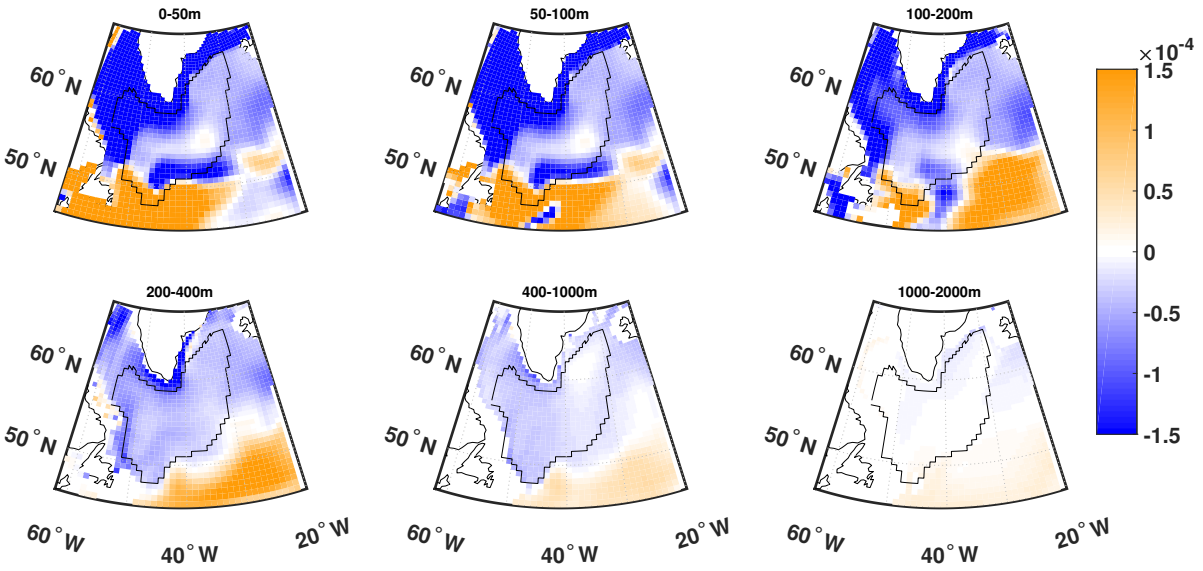

Figure 5.6.: Mean changes of freshwater $[{}^{m^3}/_{m^3} - {}^{m^3}/_{m^3}]$ at each grid point. The colour scale is restricted to emphasize the three different zones of negative, slightliy negative and positive mean changes. Averaged over all winter-differences from 1993 to 2015.

400 m, no spatial differences and a zero mean freshwater change have to be noted. Along the coast of Greenland and in the Labrador Sea, the freshwater change is negative on average, which means that in this region, an overall freshwater influx can be observed. It is not shown here that the pathway from the western Greenland coast into the Labrador and from the eastern Greenland coast into the Irminger Sea have an average freshwater influx which is one order of magnitude larger than the limits of the colormap in Fig. 5.6. In the centre of the SPG, a broad band of smaller (but still negative) mean changes can be identified. South of 50 °N, the differences are positive, which means that on average the import of more saline water takes place.

5.2. Influence of saltwater volume fluxes on the freshwater variability

Timeseries of volume fluxes

To characterize the volume flux of freshwater, three contributions are taken into account: two advective terms which describe the transport of volume $G^{\eta,\mathrm{conv}}$ and of salt itself $G^{S,\mathrm{adv}}$, and an diffusion term $G^{S,\mathrm{diff}}$. Only the timeseries for eastern and western SPG are shown (Fig. 5.7 and 5.8), which are exemplary for the different boundary currents as it has been found for the freshwater content. The two contributions to the salinity advection (cf. eq. (3.4)) are showing the same characteristics in all dimensions (latitude, longitude, depth and time) and have the same order of magnitude. Therefore, in the following, the results are exemplary presented only for $G^{S,\mathrm{adv}}$. The corresponding plots for $G^{\eta,\mathrm{conv}}$ can be found in the appendix (chapter B).

The advection term shows very low temporal variability (Fig. 5.7). From 1995-1998, where high freshwater content is found (cf. chapter 5.1), slightly stronger advection is found in the mixed layer. In 2011, when the extreme freshwater event took place, no change in the salinity advection shows up, but in 2012 the salinity transport below 200 m is decreased in the western SPG. The variability of salinity advection does not show abnormal events. Especially in the eastern SPG the transport rates are nearly constant. This also holds for the western SPG except from four years with less transport (1999, 2000, 2005, 2012) than all other years. It is noteable, that there is up to five times stronger advective transport in the deep layers than in the mixed layer. Both parts of the SPG show similar flux strength, but there is a layer of increased transport in the western SPG between 2000 m and 3000 m.
The diffusive contribution shows stronger variation on smaller scales. In the mixed layer, two years of large diffusion (1996 and 2011) are visible in Fig. 5.8. The transport velocity in mixed and deep layer are in the same range. In generall, in the eastern SPG, there the diffusion occurs to be stronger, but especially the layer between 150 m and 500 m has strong diffusive transport compared to other depth ranges. Looking at depths of 500 m to 1000 m, the pattern of diffusive transport occurs to be similar to the pattern of the freshwater changes in Fig. 5.4. It has to be noted, that diffusive transport is three orders of magnitude smaller than advective transport.

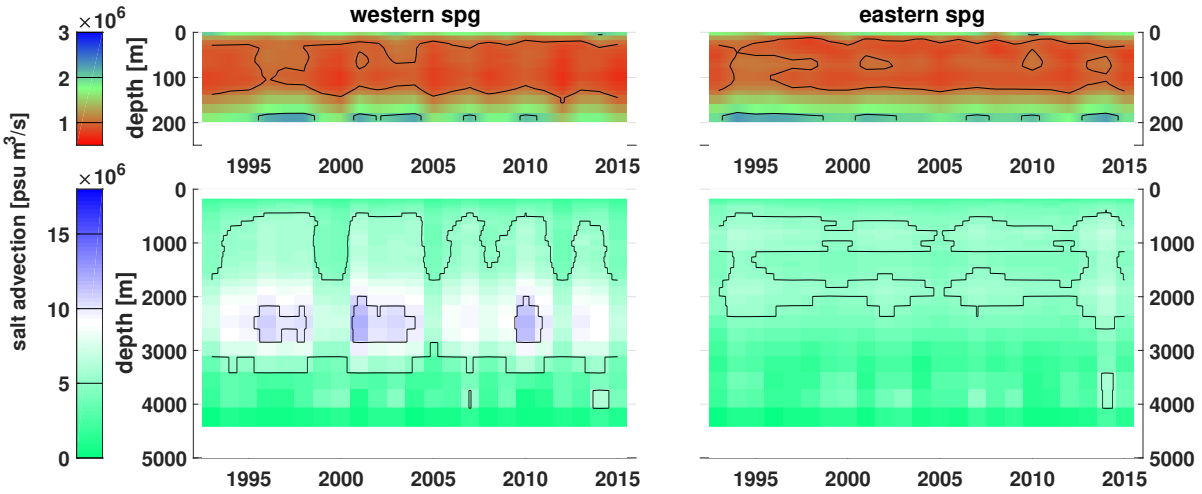

Figure 5.7.: Winter timeseries for advective salt transport $G^{S,\mathrm{adv}}$ $[\mathrm{psu\,m^3/s}]$ as a function of depth and time. Averaged over the western and eastern SPG, respectively. Upper panels show upper 200 m, lower panels show 200 m – 5000 m.

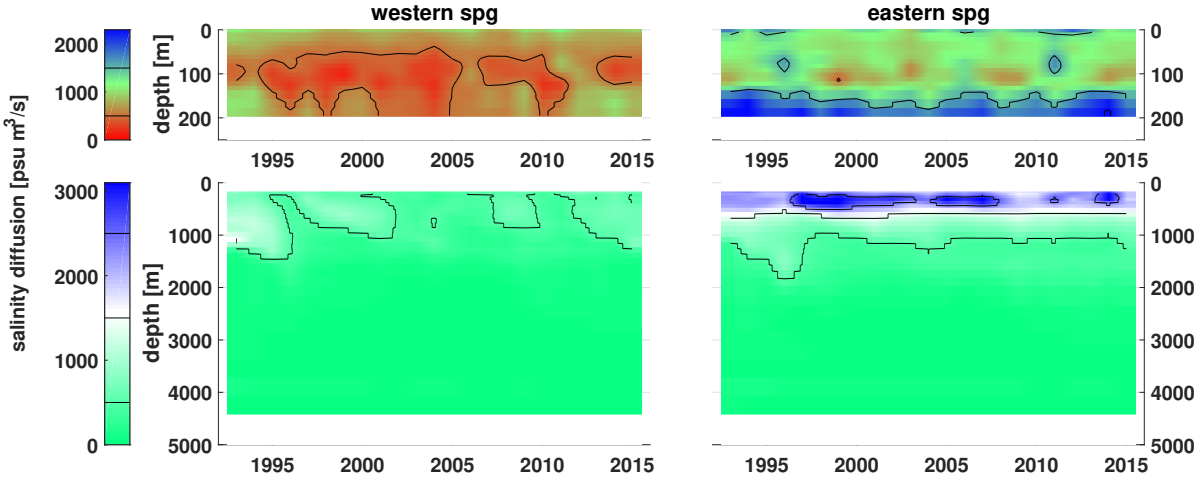

Figure 5.8.: Winter timeseries for diffusive salt transport $G^{S,\mathrm{diff}}$ $[\mathrm{psu\,m^3/s}]$ as a function of depth and time. Averaged over the western and eastern SPG, respectively. Upper panels show upper 200 m, lower panels show 200 m – 5000 m.

Correlation Analysis

How strong is the influence of the volume flux terms onto the freshwater variability? To find an answer to this, the correlation between the two flux components (advection and diffusion) and freshness has been calculated for each gridpoint in the investigated region. This is shown as a map of correlations in Fig. 5.9 and 5.10.

Inside the SPG, the advection term shows an overall high positive correlation in depth of 50 m to 200 m (Fig. 5.9). At the same depths, the correlations surrounding the SPG are negative. With increasing depth, the correlations are decreasing towards zero. In the 1000 m to 2000 m-layer, negative correlations occure surrounding the Reykjanes Ridge. The correlation between diffusion and freshness is especially strong in the mixed layer (cf. Fig. 5.10). While in the upper 100 metre high positive correlations can mainly be found in the western SPG and directly at the coast of Greenland, in the 100 m to 200 m-layer, this signal spreads into the eastern SPG. In the total mixed layer, strong negative correlations of diffusive salt flux and freshness are found at the Canadian coast. In depth of 200 m to 400 m, coefficients deviating from zero are mainly found outside the gyre following the NAC. In 400 m to 1000 m, again a strong positive correlation signal occurs in the western SPG. It vanishes in the subjacent layer.

Correlations larger than 0.4 reach a significance level of 95 %. This criterion is a strong filter for the correlations between advective fluxes and freshness (cf. Fig. 5.11). From the remaining signal, above all I can derive a separation between inside and outside the gyre, where there are positive correlations inside the gyre and negative ones outside. Strongest correlations are found in 50 m to 100 m depths following the Labrador Current into the SPG. The negative correlation branch around the Reykjanes Ridge occurs to be statistically significant.
The correlation patterns of the diffusive flux component and freshness described above, can be found as well after the application of the significance criterion (Fig. 5.12).

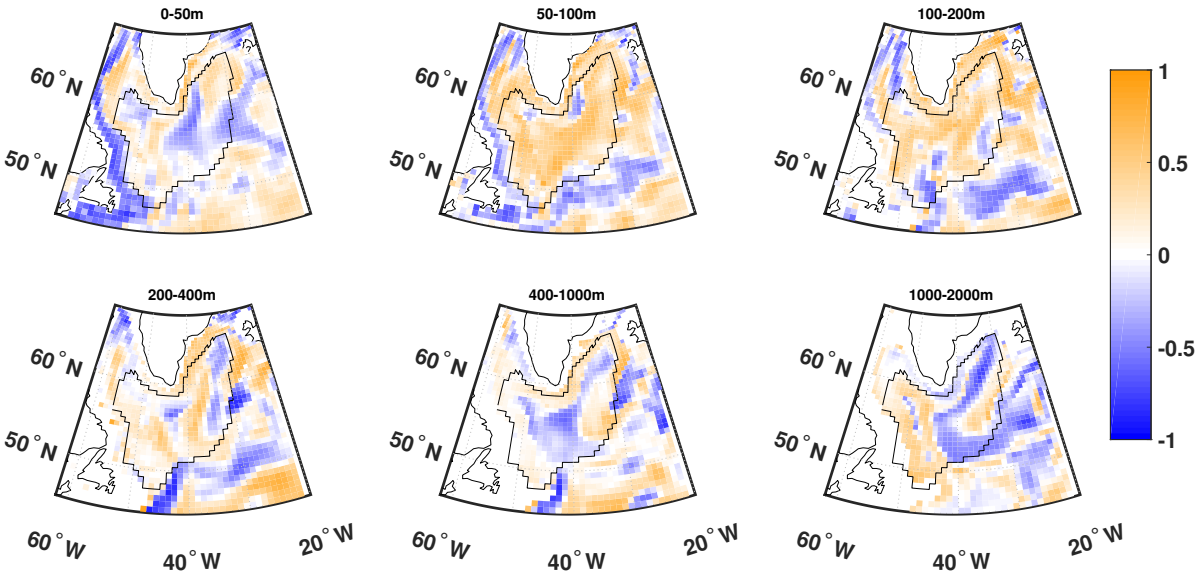

Figure 5.9.: Correlation of advective salt transport ($G^{S,\mathrm{adv}}$ $[\mathrm{psu\,m^3/s}]$) with the freshness for all winters from 1993 to 2016 in different depth layers. The remaining significant correlations are shown in Fig. 5.11.

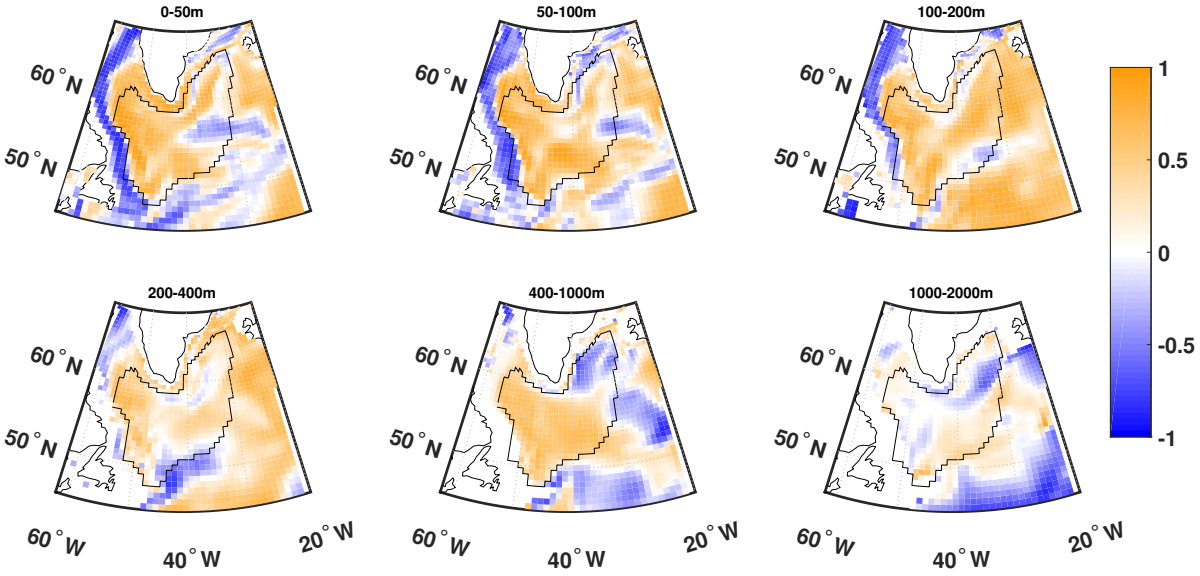

Figure 5.10.: Correlation coefficients of diffusive salinity transport ($G^{S,\mathrm{diff}}$) $[\mathrm{psu\,m^3/s}]$ with the freshness for all winters from 1993 to 2016 in different depth layers. The remaining significant correlations are shown in Fig. 5.12.

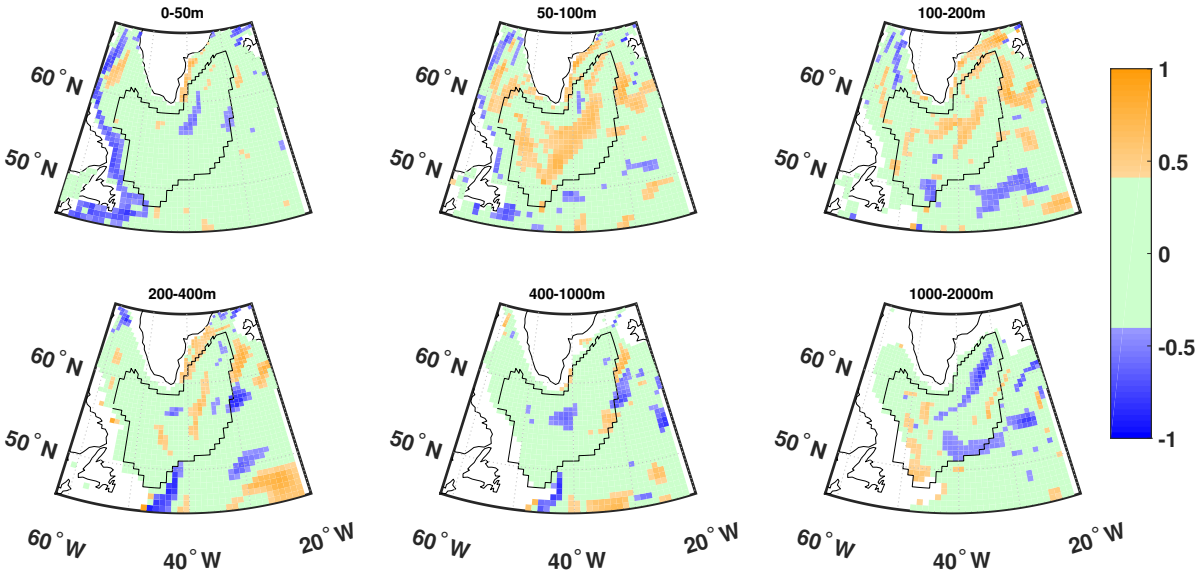

Figure 5.11.: Statistically significant correlation coefficients of advective salt transport ($G^{S,\mathrm{adv}}$ [psu m^3/s]) with the freshness for all winters from 1993 to 2016 in different depth layers.

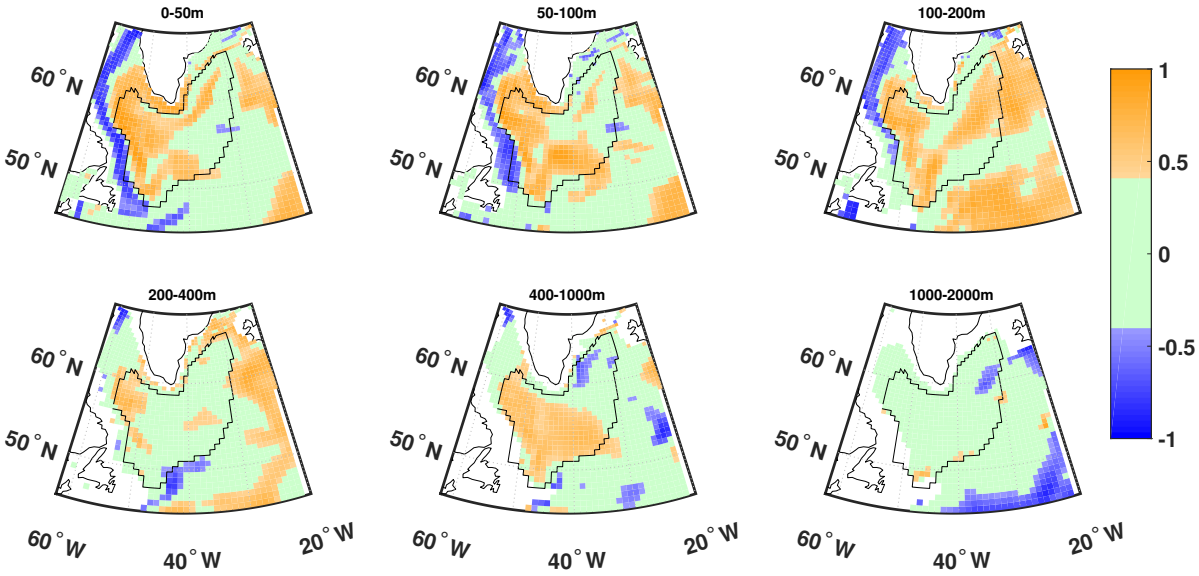

Figure 5.12.: Statistically significant correlation coefficients of diffusive salinity transport ($G^{S,\mathrm{diff}}$) [psu m^3/s] with the freshness for all winters from 1993 to 2016 in different depth layers.

Since the freshwater variability is strongest in the mixed layer (0 m – 200 m), the correlation with the volume flux terms in this layer will be investigated in more detail. According to the regions defined in chapter 4.3.3, the mean timeseries of freshness and advection components in each region can be compared to each other. This has been done for two different depth ranges (0 m – 50 m and 0 m – 200 m) in Tab. 5.1.

region	$G^{S,\mathrm{adv}}$		$G^{S,\mathrm{diff}}$	
50m				
total SPG	0.14	(47.11)	0.66	(99.93)
western SPG	0.12	(40.98)	0.85	(99.99)
canadian coast	0.10	(36.37)	0.90	(99.99)
central SPG	−0.14	(48.91)	0.67	(99.95)
eastern SPG	−0.14	(46.54)	0.36	(90.48)
greenland coast	0.18	(57.74)	0.03	(11.15)
200m				
total SPG	0.56	(99.49)	0.65	(99.92)
western SPG	0.34	(89.24)	0.63	(99.88)
canadian coast	0.37	(91.51)	0.86	(99.99)
central SPG	0.58	(99.59)	0.64	(99.90)
eastern SPG	0.52	(98.92)	0.61	(99.79)
greenland coast	0.46	(97.12)	0.29	(81.48)

Table 5.1.: Correlations between the volume transport terms of salinity ($G^{S,\mathrm{adv}}, G^{S,\mathrm{diff}}$) and freshness in the surface layer (50 m) and in the mixed layer (200 m) in different SPG regions. The values are the correlation coefficients, the values in brackets give the significance level of the correlation in %. Significant correlations are marked gray.

The correlations of the advective salt transport terms with freshness are increasing with depth. In the surface layer (top 50 m), they do not show significant correlations with freshness, but including the total mixed layer (top 200 m) the correlations in the eastern SPG are found to increase strongly towards a coefficient of ∼0.5.
The diffusion term strongly correlates with freshness in the western SPG. There, the coefficients are slightly decreasing from the surface to the mixed layer. In the eastern SPG, the correlations between the two timeseries are not significant in the surface layer, but nearly double in the mixed layer.

5.3. Influence of freshwater surface fluxes on the freshwater variability

Timeseries of surface fluxes

The timeseries of the total freshwater surface fluxes in different regions of the SPG (Fig. 5.13) show fluctuations during the whole investigated period. The variability is similar in all regions and shows a period of zero fluxes from 1998 to 2001. Before this phase, peaks of years with high surface fluxes are alternating with years of zero flux. These fluctuations are covarying with the freshness timeseries. After 2002, the surface flux is oscillating around $1 \times 10^{-8}\,\mathrm{m/s}$ in all regions. Although the freshness variability after 2000 is decresed as well, still covariation between surface fluxes and fresness can be seen. The freshwater peak in 2011 is accompanied by a freshwater flux peak in 2010 in the western SPG and in the Canadian coastal region.

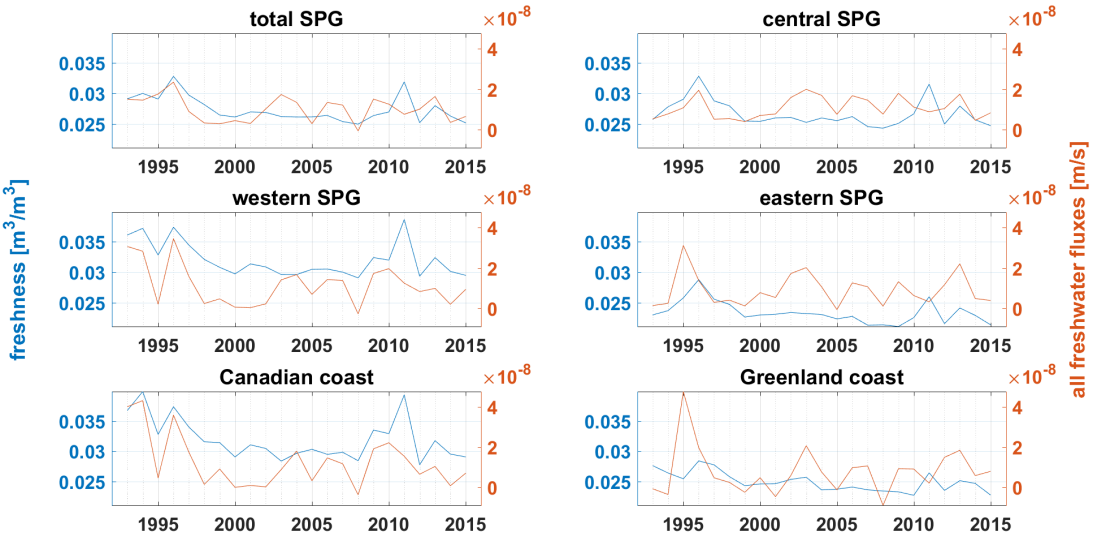

Figure 5.13.: Timeseries of total freshwater surface fluxes (red) during winter from 1993 to 2016 for the six different regions given in the supertitles. For comparison, also the timeseries of surface freshness in the top 25 m (blue) are shown.

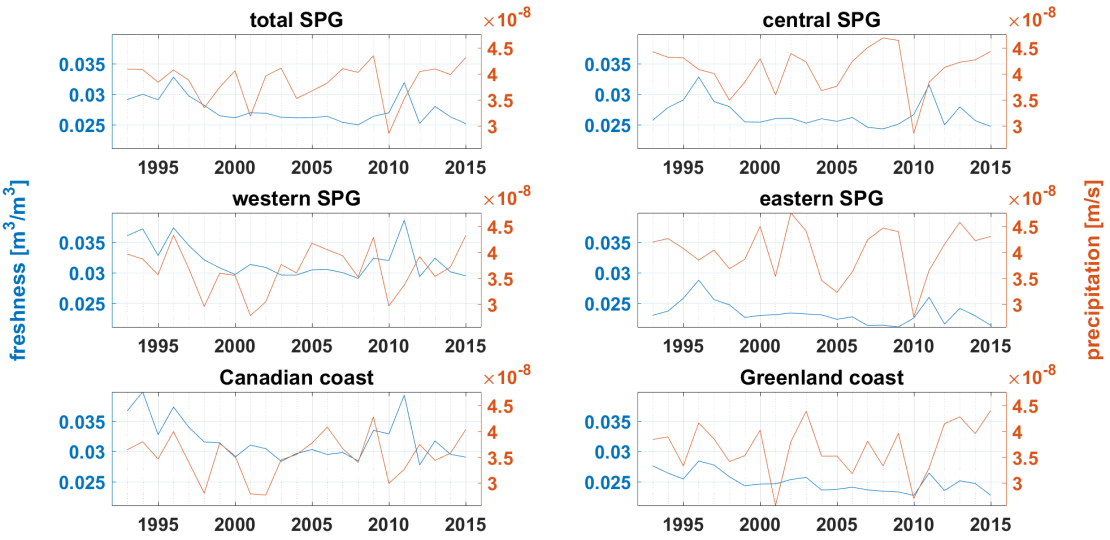

Figure 5.14.: Timeseries of precipitation (red) during winter from 1993 to 2016 for the six different regions given in the supertitles. For comparison, also the timeseries of surface freshness in the top 25 m (blue) are shown.

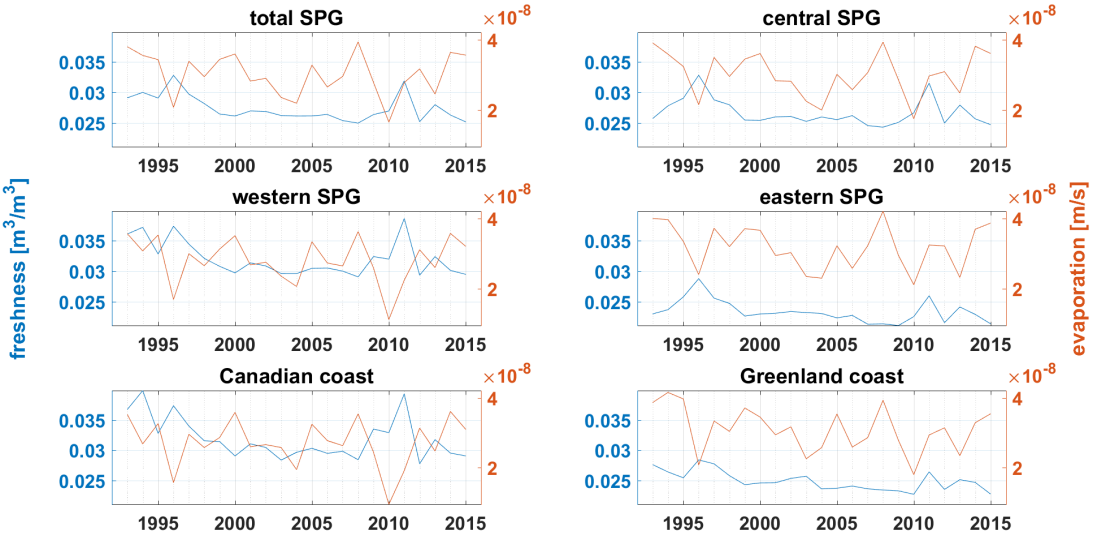

Figure 5.15.: Timeseries of evaporation (red) during winter from 1993 to 2016 for the six different regions given in the supertitles. For comparison, also the timeseries of surface freshness in the top 25 m (blue) are shown.

The precipitation curves (Fig. 5.14) show a different behaviour. No phases can be identified, but in 2010 especially low precipitation is found in all regions of the SPG. The precipitation varies between $3 \times 10^{-8}\,\mathrm{m/s}$ and $4.5 \times 10^{-8}\,\mathrm{m/s}$ during 1993 and 2016. It is noticeable, that the covariation of precipitation and freshness is higher in the first years of the investigated period. Since 2000, covariation strongly decreased. Also the evaporation timeseries (Fig. 5.15) do not show phases or a specific pattern. But it is noticeable, that the peaks of the evaporation pattern coincide with the minima of the freshness curve and vice versa. An event of especially low evaporation happens in 2010, it occurs in all regions.

Correlation Analysis

To quantify the connection between the surface fluxes and the freshwater variability, the correlation coefficients of the time series have been calculated for each region. They are shown in Tab. 5.2. The non-significant correlations are even more decreasing with increasing depth for all three evaluated fluxes (total surface fluxes, precipitation and evaporation). The only correlation coefficients which are found to be significant are between freshness and the total surface fluxes in the western SPG. These values are constant over the mixed layer depth. Both, precipitation and evaporation, do not show significant correlations with freshness inside the gyre.

region	total surface fluxes		precipitation		evaporation	
50m						
total SPG	0.45	(97.03)	−0.09	(33.32)	−0.17	(57.07)
western SPG	0.65	(99.92)	0.06	(22.61)	−0.23	(70.87)
canadian coast	0.78	(99.99)	0.06	(21.82)	−0.36	(90.55)
central SPG	0.12	(41.74)	−0.25	(74.21)	−0.27	(78.80)
eastern SPG	0.25	(74.27)	−0.13	(44.94)	−0.21	(67.05)
greenland coast	0.08	(29.27)	0.21	(66.40)	0.07	(25.91)
200m						
total SPG	0.45	(96.67)	−0.03	(10.63)	−0.07	(24.94)
western SPG	0.65	(99.92)	0.09	(31.86)	−0.11	(38.11)
canadian coast	0.78	(99.99)	0.07	(24.85)	−0.25	(75.82)
central SPG	0.05	(18.88)	−0.19	(62.34)	−0.17	(57.51)
eastern SPG	0.23	(71.48)	−0.07	(23.85)	−0.14	(47.06)
greenland coast	0.08	(29.16)	0.20	(64.37)	0.12	(40.91)

Table 5.2.: Correlations between freshwater surface fluxes and freshness in different SPG regions in the surface layer (top 50 m) and the mixed layer (200 m). The values are the correlation coefficients, the values in brackets give the significance level of the correlation in %. Significant correlations are marked gray.

The spatial distribution of significant correlations can be seen in Fig. 5.16 - 5.18. Large areas of significant, positive correlation coefficients can be found following the Labrador Current and the EGC. These correlations only occure in the mixed layer (to 200 m). It is visible, that there are nearly no correlations inside the gyre, except from a point close the Newfounland coast, where the Labrador Current enters the SPG.
The precipitation does not show correlations with freshwater content in the upper 200 m. Below this boundary, there spots of negative correlations occure. Since the influx of surface forcing should not increase with depth, these correlations are probably not physical and therefore are not taken into account for the discussion.
The correlation map of freshness with evaporation (Fig. 5.18) looks very similar to the map of total surface flux correlations (Fig. 5.16) except from the sign of correlations. The change in sign can easily be explained by the negative contribution of evaporation to total freshwater fluxes. The correlations between freshness and evaporation are especially strong in the upper 100 m of the water column.

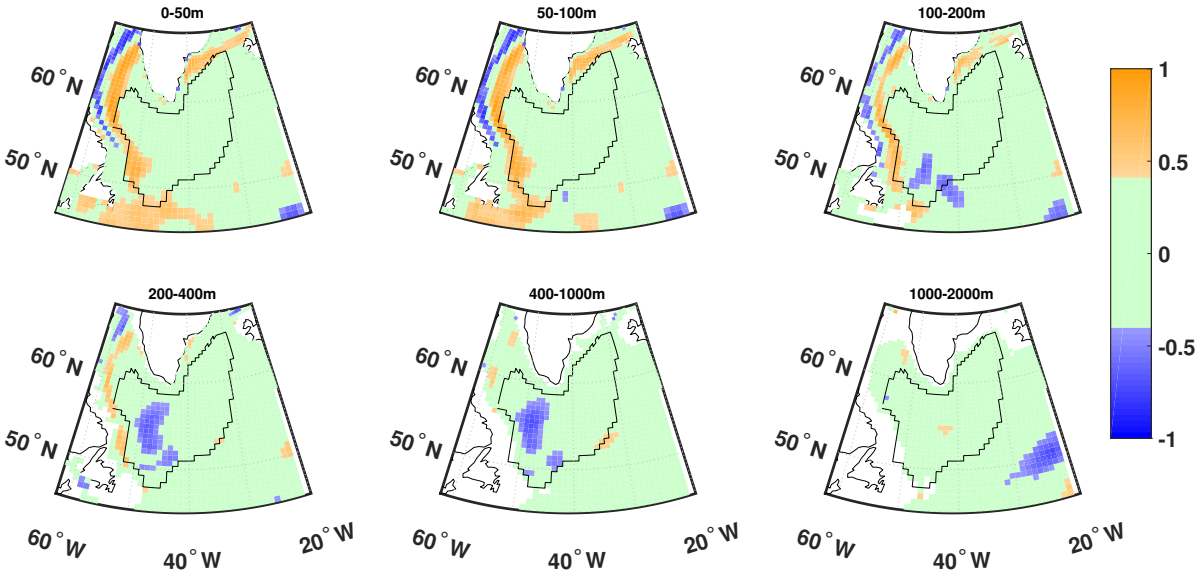

Figure 5.16.: Map of significant correlation coefficients between freshness in different depth layers and all freshwater surface fluxes. Only winter data used. The correlated timeseries reach from 1993 to 2015.

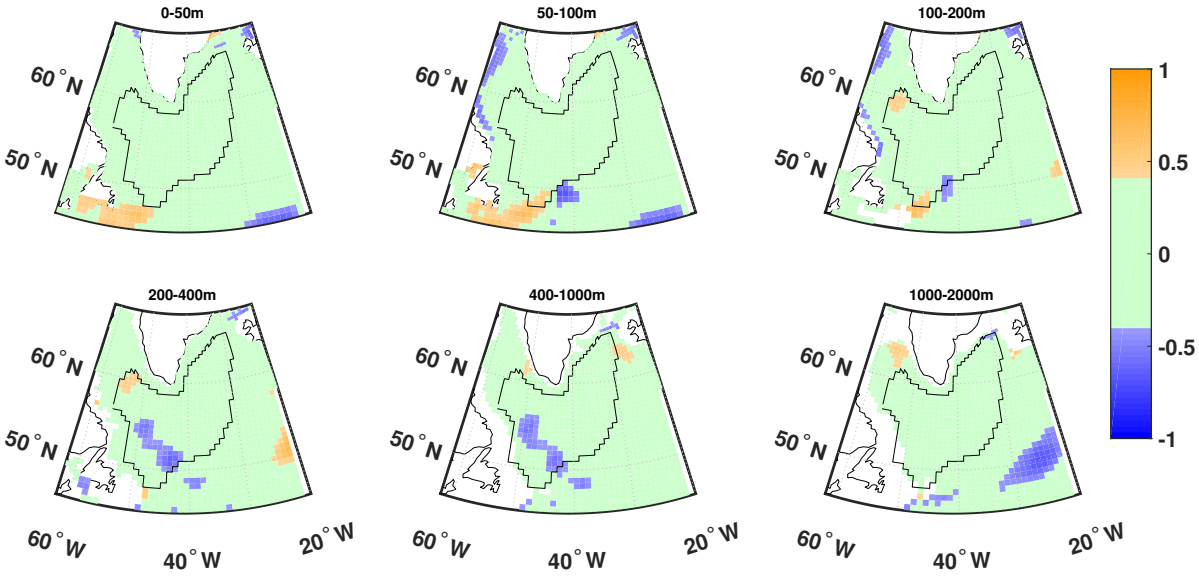

Figure 5.17.: Map of significant correlation coefficients between freshness in different depth layers and precipitation. Only winter data used. The correlated timeseries reach from 1993 to 2015.

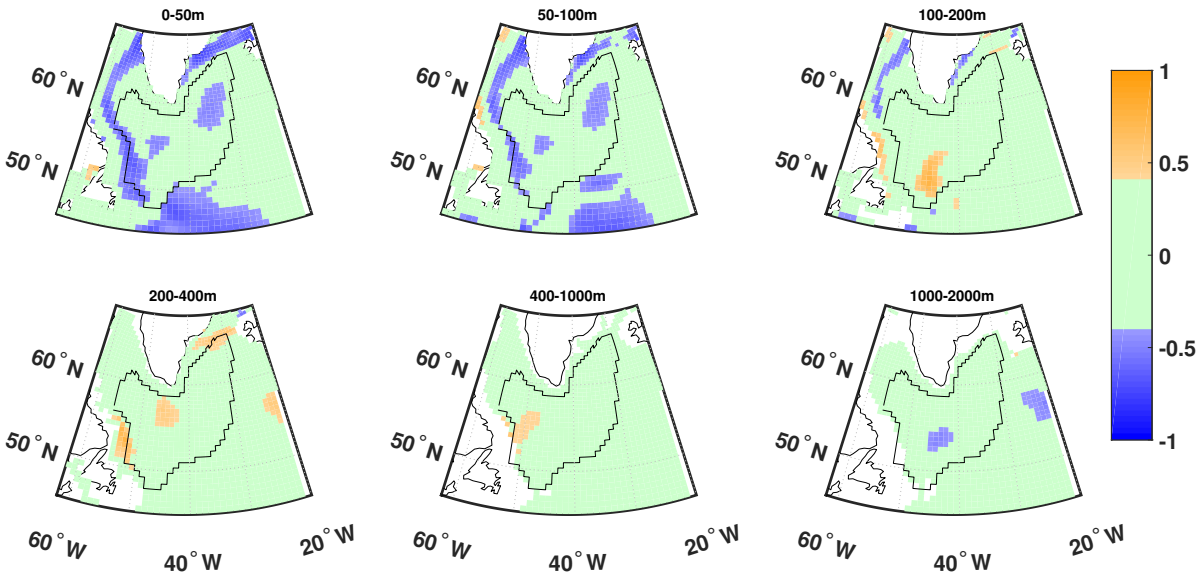

Figure 5.18.: Map of significant correlation coefficients between freshness in different depth layers and evaporation. Only winter data used. The correlated timeseries reach from 1993 to 2015.

6. Discussion

6.1. Freshwater content

From the temporal analysis of the freshness, I get the results that the content below 500 m is stable and has very low variability compared to the mixed layer (top 200 m). The freshness decreases with increasing depths, which can be explained by the lower density of freshwater compared to salty water. Also the lower variability could be a reason for the lower freshwater content, since import of surface freshwater is suppressed. In 2011, an event of strong freshness appears. It is part of a phase of increasing freshness that starts in 2009 at the Canadian coast and in the western SPG and can be found one year later in the eastern SPG as well. This phase follows on a period of constant freshness which started around 2000. In earlier years, an increasing salinity and high variability can be found. These results can be put in the context of Piecuch et al. [23], who found two phases of temperature trends in the subpolar North Atlantic. In 2004/2005, they found a switch from the increasing to decreasing temperature regime, using the same data set as has been done for this thesis. It can be concluded that an increasing temperature and an increasing salinity go together, as well as the inverse case. This could be a hint to an exchange of water masses, which can be found in the ECCO data set.

The similarity of the timeseries of the different SPG regions (Fig. 5.1) leads to the conclusion, that the western SPG is primarily influenced by the variability at the Canadian coastal boundary, which means the variability of the Labrador Current. The freshwater variability in the eastern SPG and at the northern SPG boundary also shows resemblance. For these two variables it is not to say which one is the dominant, because there is no time or intensity lag in the analysed data. Since the strength of variability is less in the eastern SPG than in the western SPG, one could conclude, that almost only the Labrador Current influences the SPG variability, whose influence decreases during the transport

through the gyre. This eastward transport has also been found by Dukhovskoy et al. [33]. Also the flow direction within the SPG implies a transport away from the Canadian coast through the western SPG towards the north-eastern SPG. At this point, a recirculation along the Greenland coast towards the Labrador Sea (Fig. 4.6) is found. However, in the ECCO data set no time lag is present between western and eastern SPG, which means that an interaction between both regions needs to be instantaneous on the time scale of one winter. The mean flow velocity in the top 200 m is between 0.03 $^{m}/_{s}$ and 0.05 $^{m}/_{s}$ which refers to 200 $^{km}/_{winter}$ – 400 $^{km}/_{winter}$, which is less than half of the extension of the SPG ($\sim$ 1000 km). So, possibly, there is also an overlying impact, which influences both regions.

Although the spatial analysis does show a homogeneous distribution of freshwater within the SPG (Fig. 5.3), it has to be noted, that in the top $\sim$1000 m, a higher freshwater proportion at the Canadian coast and in the western SPG can be seen. It is likely, that the higher salinity in the eastern part results from weak interactions with the NAC as eastern boundary current. Inside the gyre, the salt then is transported towards the Greenland coast. Another possible explanation takes the higher freshwater variability in the western SPG into account: While the Labardor Current triggers the variability at the Canadian coast (which also influences the western SPG), the eastern SPG is not affected by the signals imported from the Labrador Sea.

6.2. Freshwater variability

The results of the temporal analysis of freshwater changes emphasize the conclusion already drawn above. Especially two phases of high variability can be named additionally. No variability occurs during 2000-2010, where there is no salinity trend in the SPG as well. In the intermediate layers (below 200 m), freshwater variability can be found as slow downward propagation of mixed layer input. Below $\sim$ 2500 m, there is no variability present on the investigated scales.
From the spatial analysis of the interannual freshwater changes, two regions in the SPG are identified. Both regions show negative mean freshwater changes, which implies that on average the freshwater content in every year is higher than in the previous year. This effect is stronger by a factor of $\sim$ 3 in the Labrador Sea and at the coast of Greenland

than in the central SPG. To summarize, the total subpolar North Atlantic has been freshening from 1993 to 2016, with a stronger intensity found in the Labrador Sea.

6.3. Volume flux

Advective salinity transport

The advective fluxes of volume and salt show up to be almost constant in time. The stronger top layer (top 50 m) variability of advection does not show correlations with the freshwater in the same layer. Therefrom, it can be concluded, that the salt advection does not influence the freshwater variability in the uppermost 50 m of the SPG.
Including the whole mixed layer depth, there are positive correlations distributed over the total investigated area. Two contiguous areas of high correlations can be identified: (1) The Labrador Current and its expansion into the SPG: This is the region which is found to be an "inflow" region into the SPG by other authors [46, 79]. (2) A band of correlations in the eastern SPG reaching from the southwest towards the northeast: This band totally follows the flow direction in the SPG and is responsible for intragyre spread of water masses.
Comparing the SPG with its surrounding regions, it is noteable that the correlations inside the gyre are positive, while the outer correlation coefficients are negative. From physical intuition, one expects higher salinity advection corresponding to lower freshness, which results in negative correlations. How is an occurence of positive correlations possible? A variation of the salinity transport term could be due to variation of the salt content, or due to variation of the transport velocity. While an increased salt component leads to lower freshwater content, an increased velocity of the advective transport results in higher freshwater content (because the salt is carried away). From this, one could draw the conclusion that inside the gyre more fresh water is transported, while outside the gyre more saline water is carried along and causes salinisation.
However, in the 1000 m – 2000 m-layer, a branch of negative correlations can be found around the Reykjanes Ridge. From the argumentation above, negative correlations imply influx of more saline water. This could be easily explained by the above mentioned higher salinity in deeper layers. Another possibility is the import of salt into these layers from outside the gyre or from other layers. This could be induced by deep convection, which has been described by several authors [80–82] for the investigated time period in

these depths. Import from other regions is also found by a deep branch of the NAC surrounding the Reykjanes Ridge at the eastside which follows exactly the pathway where the correlations are found [83].
Between 200 m and 1000 m, hardly any connection between freshness and salinity advection can be identified. From the model (eq. (3.3)), only three contributions can influence the freshwater content: advective fluxes, diffusive fluxes and surface fluxes. The surface fluxes do not influence the layers below 200 m, which has been shown in chapter 5.3. Diffusive fluxes are three orders of magnitude smaller than the advective fluxes (Fig. 5.7, B.1 and 5.8). So the transport of freshwater is expected to be mainly influenced by advection. This is reflected in the overall constant timeseries of both, freshness and salinity advection below 200 m. Possibly, this stability at the same time explains the very low correlation between the two variables: Since there are no strong, overlying fluctuations, small fluctuations are not negligible. Hence, although the freshwater content is determinded by advection, the freshwater variability could be determined by diffusive or surface forcings.

Diffusive salinity transport

Although the salinity diffusion only has a small contribution to the total transport compared to advection, from the correlation analysis it seems to be the most important driving factor for freshwater variability. This can be explained by the turbulence contained in the diffusion term [60]. Advective transport by mesoscale eddies and vertical convection are part of the turbulence and therefore of the diffusion term. From the correlation analysis between freshness and diffusive salinity transport, three layers can be identified which show different regions of correlation (0 m – 200 m, 200 m – 400 m, 400 m – 1000 m).
In the mixed layer (top 200 m), as for the advective flux, a differentiation between positive signs inside the gyre and negative signs following the Labrador coastal current has to be made. With the same argument as above, it can be reasoned that the correlations inside the SPG result from higher flux rates instead of higher salinity. Thus, inside the gyre most of all freshwater is transported. Looking at the correlation map (Fig. 5.12), one finds most and strongest correlations reaching from the tip of Greenland to the southermost edge of the SPG covering the total western SPG. A reason for this could be fresh river runoff from Greenland, which causes a gradient of salinity and therefore

enhances diffusion (which should be proportional to the concentration difference of salt). Additionally, input of cold and fresh water causes eddies to develop [83–85].
In the lower mixed layer (100 m – 200 m), the correlation signal detaches from the Greenland tip and spreads into the eastern SPG. This fits to the propagation of freshwater signals inside the SPG found by Dukhovskoy et al. [33].

Between 200 m and 400 m depth, there are strong correlations between salinity diffusion and freshness along the NAC. Probably, they are also the result of eddy transport, since the NAC transports water with different hydrgraphical properties than found in the subpolar North Atlantic. The differences in salinity and temperature combined with different velocities of the water masses lead to diffusive mixing and eddy formation [86, 87].

In depths of 400 m to 1000 m, again in the total western SPG high correlations between freshness and salinity diffusion are found. But the shape of the correlation area looks different from the shape found in the mixed layer. Perhaps, this originates from a current which has been found in observational data in "mid-depths" ($\sim$ 700 m) [88]. This flux is found as a recirculation inside the SPG branching off the major flow direction at the southern end of the SPG towards the Labrador Sea [88–90].

Another indication, that the diffusion term reflects the variability of freshwater is the strong diffusion event in 2011, which comes along with the high freshening in this year.

6.4. Surface fluxes

The low correlations between freshwater surface fluxes and freshness shown in Tab. 5.2 indicate, that the forcing of freshwater variability is mainly due to volume fluxes. Nevertheless, the total surface fluxes show high correlation values in the western SPG in the mixed layer (top 200 m), which are not reflected in the precipitation nor in evaporation. This leads to the conclusion, that the third term contributing to the total freshwater fluxes - the river runoff - causes these correlations.
The spatial distribution (Fig. 5.16) provides information on where the surface fluxes correlating with the freshwater variability come from. The significant correlations are

found along the EGC and the Labrador Current and enter the SPG close to the Newfoundland coast. The river runoff contributing to the Labrador Current can come from Canadian continental shelf and Greenland rivers. The EGC is mainly fed by waters from the Arctic and from Greenland. So, all contributing flows are from regions which are covered by ice during most of the year. Probably, runoff from melting ice accounts for a large proportion of the total inflows.
The precipitation does show extremely low connection to freshwater variability. Comparing both timeseries to each other (Fig. 5.14), in the western SPG, a covariation at the beginning of the investigated period (1993-1998) shows up. It vanishes in the following years and even the event of extremely low precipitation in 2010 is followed by a year of extremely high freshness. In the correlation map, no impact of precipitation onto freshness is found (Fig. 5.17). So, precipitation as a driving force for freshwater variability can be rejected with high probability. On shorter time scales, the precipitation could have greater impact, but this question has not been analysed here.
This does not hold for evaporation. Although the correlation values inside the SPG are very low (Tab. 5.2), the correlation map shows a strong connection to freshwater variability along the Labrador Current and the EGC, as well as a spot in the north-eastern SPG (Fig. 5.18). The rate of evaporation is mainly depending on the available heat and therefore on the latitude. However, it is unexpected that evaporation is influenced by oceanic currents. This means that the temperature difference between oceanic currents and the atmosphere is so large that it has significant effects on evaporation. This in turn implies that the temperature variations within the currents are strong and not in equilibrium with the ambient temperature, indicating external inflows of particularly cold (or warm) water. In this case, it is inflows of cold water, since the correlations are negative (high freshness correlates with low evaporation). In conclusion, the correlation between freshness and evaporation along the Labrador Current and the EGC supports the thesis that the currents import cold, fresh water. It cannot be reasonably assumed that evaporation could affect the freshness.

It is important to note that these results have to be seen in contrast to findings by Boyer et al. [24] and Josey and Marsh [25] which both find precipitation (and evaporation) to determine the subpolar freshwater variability until the mid 1990s.
A possible explanation for the fact that the results found here do not match with earlier studies is that the near-surface freshwater content was mainly determined by precipitation-

evaporation until $\sim$ 2000. This assumption also takes into account the strong covariation of freshness and precipitation in the late 1990s, which has been found in the ECCO data set as well. However, with an increase of melt water from Greenland and from the Arctic oceans, inputs from the cryosphere and land runoff became increasingly dominant and also determined freshwater variability in the following years to such an extent that even particularly low amounts of precipitation have no effect on the freshwater content of the subpolar North Atlantic.

6.5. Summary

The freshness in the SPG has been found to be drecreasing from 1993 to $\sim$ 2000, followed by a period of stagnation in the early 2000s. Starting around 2010, the freshwater content is increasing in the SPG. An overall freshening of the subpolar North Atlantic in the investigated time period could be shown (Fig. 5.6).
To address the initial question of this thesis, I compare the freshwater variability to the heat content variability found by Piecuch et al. [23]. Both variables, freshness and heat content, show two phases in the time period from 1993 to 2016: the heat content increases (the freshness decreases) until 2004/2005, afterwards both change their slope. In the freshness, also a third phase from approximately 2000 to 2009 has been identified, in which the slope is close to zero and very low variability is found. This phase is not explicitely described for the heat content.

From the analysis of the single terms contributing to the salinity conservation (eq. (3.3)), it can be inferred that salinity advection is volumetrically the largest component of salinity transport. Nevertheless, the diffusive salinity transport (which includes eddy advection and convection) dominates the freshwater variability in the mixed layer (uppermost 200 m) and in the 400 m – 1000 m-layer. Probably, eddy formation is the main source of this variability, which is a hint to input of external water masses influencing the freshwater content.
The surface forcing only has a connection to the freshness in the western SPG, where there is import of water from the Labrador Current expected. The evaporation and precipitation over the SPG are not influencing or influenced by the freshness in the SPG, but strong correlations between evaporation and freshness along the Labrador Current

and the EGC reveal that the temperature of the imported freshwater has to be lower than of the ambient air and ocean. Since there are correlations in the total surface fluxes which cannot be found in precipitation and evaporation data in the SPG, the third, missing component (river runoff) should be responsible for this connection.
From this I conclude, that melting ice imports from the Arctic, the Canadian coastal shelf and Greenland have a large impact on the Labrador Sea freshwater variability, which is transported into the SPG via the Labrador Current and turbulent eddies. Before 2000, the influence of river runoff probably was smaller, since the timeseries of precipitation covary with freshness during the 1990s. So, it is likely that since the early 2000s the impact of river runoff increased. This led to a reversal in the freshening behaviour of the SPG. Due to the slow response of the ocean to external forcings, first a phase of freshness stagnation during the 2000s is initiated, which then slowly strengthens into freshening of the SPG since 2010.

Also Piecuch et al. [23] searched for the mechanisms that lead to a trend reversal of the oceanic heat content in the subpolar North Atlantic. They state, that it is due to heat advection by midlatitude ocean circulation. Changes in the deep and intermediate vertical overturning circulation are excluded as possible reason for the trend inversion, but horizontal gyre transports are named as primary contribution. Anomalous horizontal gyre circulations are found to be driven by the local wind stress curl.
A differentiation into horizontal and vertical circulations has not taken place in the present thesis. For volume fluxes, I only examined the horizontal components. This is justified by the proposition of Piecuch et al. [23]. However, they do not make any difference in the type of transport, which was the main focus here.

In the subpolar North Atlantic, an important part of the AMOC takes place, since here the thermohaline circulation is driven by atmospheric cooling [91]. Temperature and salinity are determining the density distribution and therefore the stability of water columns. Changes in one or both of these variables would cause changes in the circulation pattern of the whole region and corresponding boundary regions. This also significantly influences atmospheric fluxes. Therefore, the investigation of freshwater in this region makes an important contribution to the debate on the consequences of climate change. The results found here demonstrate that the influence of freshwater inflows increased so much since $\sim$ 2000 that precipitation only has subordinate impact. This is in contrast to

studies from earlier years [24, 25], which confirms the assumption that a new freshwater source has a large contribution to the variability in the SPG. Its hydrographical properties are characterized by lower salinity and temperature than before. The described features lead to the assumption, that melt water from Greenland, Canada and the Arctic accounts to be the source. However, the input causes an overall change of the subpolar North Atlantic towards lower salinity in the upper layers (200 m) on timescales of only a few years (1-2 decades).
The long-term consequences and climate feedback cannot be estimated, since no biological or atmospheric investigations have been carried out yet.

6.6. Outlook

So far, no cause for the freshwater event in 2011 could be found. The signal is also reflected in the time series of diffusive transport and evaporation, but these variables both are probably influenced by the freshwater amount and not vice versa. Possibly, the seasonality was shifted in this year, so that other months would have been representative for the "winter" 2011.

To confirm the major role of melting ice fluxes in the freshwater surface fluxes, data about actual river runoff needs to be tested. Unfortunately, in the ECCO data set this data is not available with a good resolution. So, other data sets could be analysed. Another possible test is the comparison of freshness in the subpolar North Atlantic with an index characterizing the ice melting. [1]

Another interesting question concerns the pathways of freshwater. Did they change due to the import of melting ice water? Does the cold water cause more convection or does the temperature difference between subtropical and subpolar North Atlantic decrease, which causes a decline of the AMOC? This query cannot be answered here, since diverse investigations lead to various results. It is also possible, that both scenarios occur on different time scales. A study of Våge et al. [80] reports the onset of deep convection in

[1] Actually this has been done with the ice volume index by Schweiger et al. [92]. The correlation minimum between freshness and ice-volume is 0.54 in the central SPG, the maximum (0.74) can be found at the Greenland coastal region. All regions show correlations with a significance level $> 99\,\%$. The analysis is not mentioned above, because the data is not part of the ECCO data set.

the SPG in winter 2007/2008. A similar approach has been published by de Jong and de Steur [82], who reported that in winter 2014/2015 mixed layer depths of up to 1400 m occured in the eastern SPG and Irminger Sea, which are related to "exceptional deep convection" [82] in the same winter. Nevertheless, they also state, that this event was probably caused by atmospheric forcing (instead of river runoff).
At the same time, Thornalley et al. [49] find a declining Labrador Sea convection during the last 150 years, which they assume to be due to enhanced ice melting on Greenland and in the Arctic seas.
Another study by Holliday et al. [34] observed changes in ocean circulation due to unusual wind patterns, which cause transport of Arctic freshwater from the western boundary to the eastern subpolar North Atlantic. This leads to extreme freshening of the eastern basins from 2012 to 2016 and a slowing of the NAC.
These results show, that the ongoing research agrees that there is an overall change in flows. However, it is not clear yet, what triggers these changes and what consequences are to expect on which time scales. To find the answer(s), ongoing investigations are needed.

Additionally to the description of the oceanographic changes, atmospheric forcings and their impact on the variability could be examined. Especially mixed layer properties are often found to be influenced by wind-stress curl or atmospheric oscillation indices which quantify the pressure variability over the North Atlantic (for example the NAO,or the East Atlantic Pattern (EAP)). Here, only atmospheric forcings which are explicitely linked to freshwater have been analysed, since they are part of the ECCO data set.

Appendix

A. List of Abbreviations

AABW Antarctic Bottom Water . . . 9

AAIW Antarctic Intermediate Water . . . 9

ADCP Acoustic Doppler Current Profilers . . . 1

AMOC Atlantic Meridional Overturning Circulation . . . 5

CTD Conductivity-Temperature-Depth . . . 1

DWBC Deep Western Boundary Current . . . 9

EAP East Atlantic Pattern . . . 61

EGC East Greenland Current . . . 11

EOF Empirical Orthogonal Function . . . 24

MITgcm General Circulation Model of the Massachusetts Institute of Technology . 13

NADW North Atlantic Deep Water . . . 9

NAO North Atlantic Oscillation . . . 30

NAC North Atlantic Current . . . 9

MOC Meridional Overturning Circulation . . . 5

PC Principal Component . . . 25

PCA Principal Component Analysis . . . 24

SPG subpolar gyre . . . 11

SSH Sea Surface Height . . . 28

WGC West Greenland Current . . . 11

B. Supplementary Figures

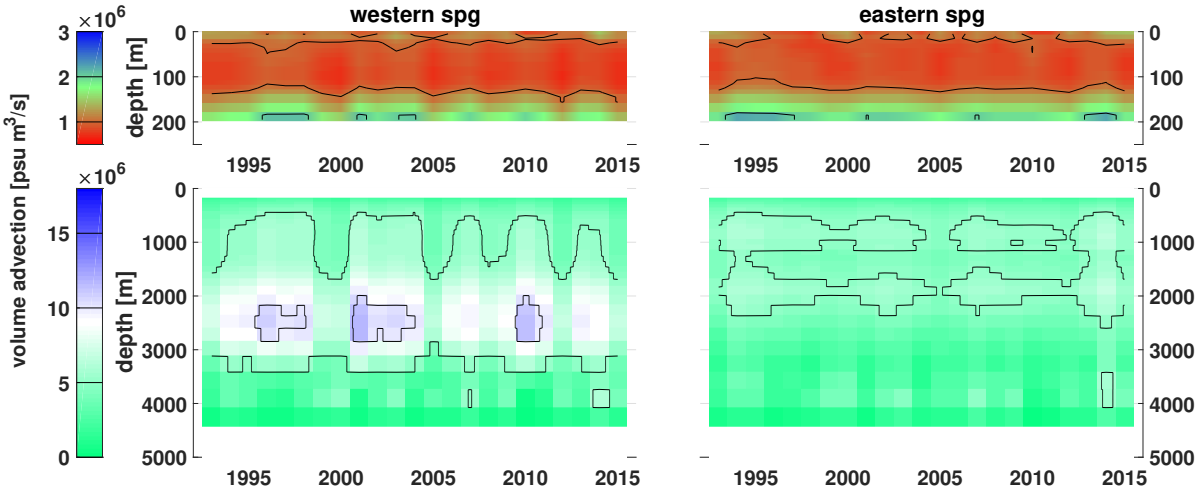

Figure B.1.: Winter timeseries for volume transport times salt content $S \cdot G^{\eta,\mathrm{conv}}$ $[\mathrm{psu\,m^3/s}]$ as a function of depth and time. Averaged over the western and eastern SPG, respectively.

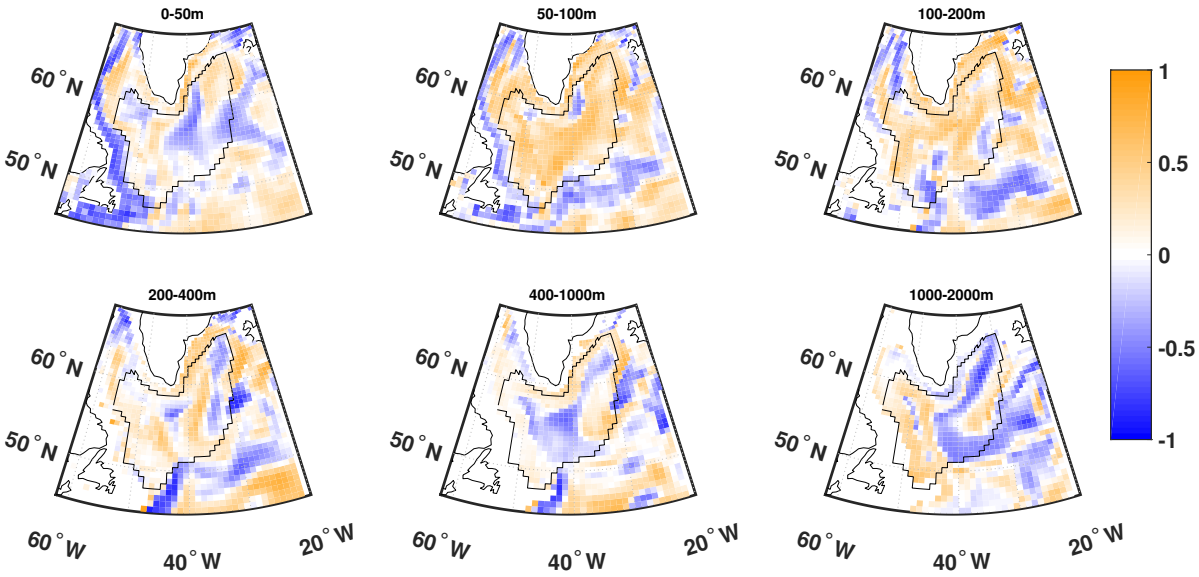

Figure B.2.: Correlation of advective volume transport times salt content($S \cdot G^{\eta,\mathrm{conv}}$ $[\mathrm{psu\,m^3/s}]$) with the freshness for all winters from 1993 to 2016 in different depth layers. The remaining significant correlations are shown in Fig. B.3.

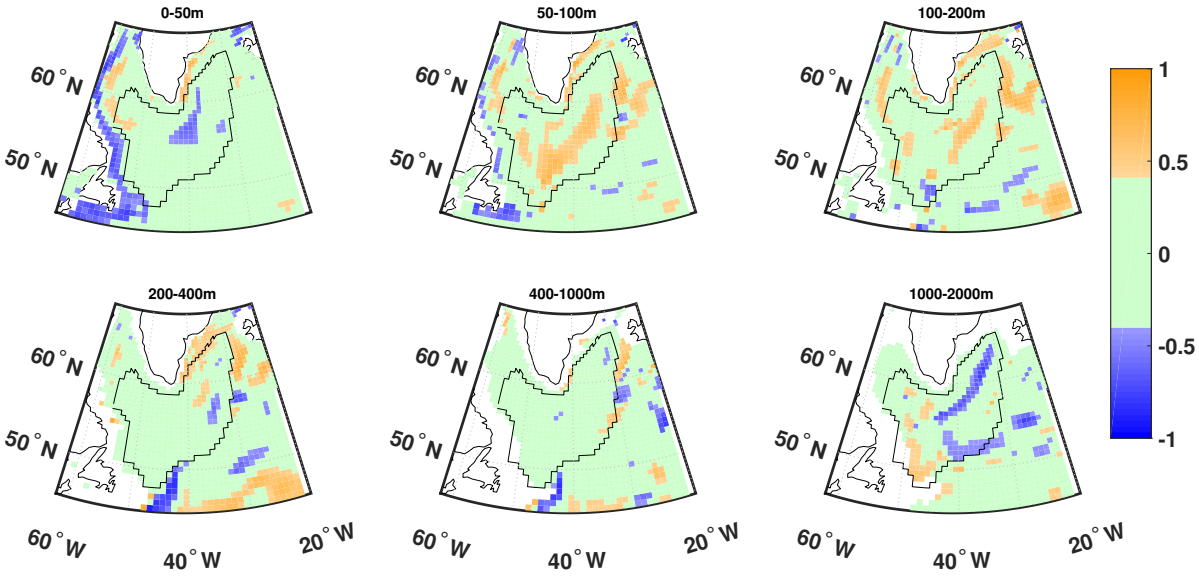

Figure B.3.: Statistically significant correlation coefficients of advective volume transport times salt content ($S \cdot G^{\eta,\mathrm{conv}}$ $[\mathrm{psu\,m^3/s}]$) with the freshness for all winters from 1993 to 2016 in different depth layers.

Bibliography

[1] C. Wunsch, P. Heimbach, R.M. Ponte, I. Fukumori, and the ECCO-GODAE Consortium. The Global General Circulation of the Ocean Estimated by the ECCO-Consortium. *Oceanography*, 22(2):88–103, 2009.

[2] G. Forget, J.-M. Campin, P. Heimbach, C. N. Hill, R. M. Ponte, and C. Wunsch. ECCO version 4: an integrated framework for non-linear inverse modeling and global ocean state estimation. *Geoscientific Model Development*, 8(10):3071–3104, 2015.

[3] Ichiro Fukumori, Ou Wang, Ian Fenty, Gael Forget, Patrick Heimbach, and Rui M. Ponte. *ECCO Version 4 Release 3*, 2017. `ftp://ecco.jpl.nasa.gov/Version4/Release3/doc/v4r3_estimation_synopsis.pdf`.

[4] Alison Duxbury and Alyn C. Duxbury. *Fundamentals of Oceanography*. McGraw-Hill Companies, 3rd edition, 1999.

[5] W. Lawrence Gates. The effect of the ocean on the atmospheric general circulation. *Dynamics of Atmospheres and Oceans*, 8:95–109, 1979.

[6] M. E. Schlesinger. *Climate-Ocean Interaction*. Kluwer Academic Publishers, 1990.

[7] Lucy J. Carpenter, Stephen D. Archer, and Rachael Beale. Ocean-atmosphere trace gas exchange. *Chemical Society reviews*, 41(19):6473–6506, 2012.

[8] A. H. Oort and T.H. Vonder Haar. On the observed annual cycle in the ocean-atmosphere heat balance over the Northern Hemisphere. *Journal of Physical Oceanography*, 6(6):781–800, 1976.

[9] H. U. Sverdrup. Wind-driven currents in a baroclinic ocean; with application to the equatorial currents of the eastern pacific. *Proc. Nat. Acad. Sci (PNAS)*, 33:319–326, 1947.

[10] Gerold Siedler, Stephen M. Griffies, John Gould, and John A. Church, editors. *Ocean Circulation & Climate: A 21st Century Perspective*, volume 103 of *International Geophysics*. Elsevier, Oxford, 2nd edition, 2013.

[11] Jaime B. Palter. The role of the Gulf Stream in European climate. *Annual review of marine science*, 7:113–137, 2015.

[12] Reindert J. Haarsma, Javier García-Serrano, Chloé Prodhomme, Omar Bellprat, Paolo Davini, and Sybren Drijfhout. Sensitivity of winter North Atlantic-European climate to resolved atmosphere and ocean dynamics. *Scientific Reports*, 9(1):13358, 2019.

[13] R. T. Sutton, D. Hodson, and P-P. Mathieu, editors. *The role of the Atlantic Ocean in climate forecasting*, Shinfield Park, Reading, 2003. ECMWF.

[14] Harry L. Bryden, Hannah R. Longworth, and Stuart A. Cunningham. Slowing of the Atlantic meridional overturning circulation at 25 degrees N. *Nature*, 438(7068): 655–657, 2005.

[15] T. Rossby. The North Atlantic Current and surrounding waters: At the crossroads. *Reviews of Geophysics*, 34(4):463–481, 1996.

[16] E. Peter Jones. Circulation in the Artic Ocean. *Polar Research*, 20(2):139–146, 2001.

[17] Bruce J. Peterson, James McClelland, Ruth Curry, Robert M. Holmes, John E. Walsh, and Knut Aagaard. Trajectory Shifts in the Arctic and Subarctic Freshwater Cycle. *Science*, 313(5790):1061–1066, 2006.

[18] W. J. Emery and J. Meincke. Global water masses: summary and review. *Oceanologica Acta*, 9(4):383–391, 1986.

[19] Peter Lemke Michael Hilmer. On the decrease of Arctic sea ice volume. *Geophysical Research Letters*, 27(22):3751–3754, 2000.

[20] D. J. Cavalieri and C. L. Parkinson. Arctic sea ice variability and trends, 1979–2010. *The Cryosphere*, 6(4):881–889, 2012.

[21] Jinlun Zhang, Ron Lindsay, Axel Schweiger, and Ignatius Rigor. Recent changes in the dynamic properties of declining Arctic sea ice: A model study. *Geophysical Research Letters*, 39(20), 2012.

[22] T. Krumpen, R. Gerdes, C. Haas, S. Hendricks, A. Herber, V. Selyuzhenok, L. Smedsrud, and G. Spreen. Recent summer sea ice thickness surveys in Fram Strait and associated ice volume fluxes. *The Cryosphere*, 10(2):523–534, 2016.

[23] Christopher G. Piecuch, Rui M. Ponte, Christopher M. Little, Martha W. Buckley, and Ichiro Fukumori. Mechanisms underlying recent decadal changes in subpolar North Atlantic Ocean heat content. *Journal of Geophysical Research: Oceans*, 122 (9):7181–7197, 2017.

[24] Tim Boyer, Syd Levitus, John Antonov, Ricardo Locarnini, Alexey Mishonov, Hernan Garcia, and Simon A. Josey. Changes in freshwater content in the North Atlantic Ocean 1955-2006. *Geophysical Research Letters*, 34(16):182, 2007.

[25] Simon A. Josey and Robert Marsh. Surface freshwater flux variability and recent freshening of the North Atlantic in the eastern subpolar gyre. *Journal of Geophysical Research*, 110(C05008):1–17, 2005.

[26] Ruth Curry, Bob Dickson, and Igor Yashayaev. A change in the freshwater balance of the Atlantic Ocean over the past four decades. *Nature*, 426(6968):826–829, 2003.

[27] J. Blindheim, V. Borovkov, B. Hansen, S.-Aa. Malmberg, W. R. Turrell, and S. Østerhus. Upper layer cooling and freshening in the Norwegian Sea in relation to atmospheric forcing. *Deep Sea Research Part I: Oceanographic Research Papers*, 47 (4):655–680, 2000.

[28] Bob Dickson, Igor Yashayaev, Jens Meincke, Bill Turrell, Stephen Dye, and Juergen Holfort. Rapid freshening of the deep North Atlantic Ocean over the past four decades. *Nature*, 416:832–837, 2002.

[29] Gilles Reverdin, Fabien Durand, John Mortensen, F. Schott, H. Valdimarsson, and W. Zenk. Recent changes in the surface salinity of the North Atlantic subpolar gyre. *Journal of Geophysical Research: Oceans*, 107(C12):SFR 11–1–SFR 11–13, 2002.

[30] S. A. Josey, M. F. de Jong, M. Oltmanns, G. K. Moore, and R. A. Weller. Extreme Variability in Irminger Sea Winter Heat Loss Revealed by Ocean Observatories Initiative Mooring and the ERA5 Reanalysis. *Geophysical Research Letters*, 46(1): 293–302, 2019.

[31] Peili Wu and Richard Wood. Convection induced long term freshening of the subpolar North Atlantic Ocean. *Climate Dynamics*, 31:941–956, 2008.

[32] Hjálmar Hátún, Anne Britt Sandø, Helge Drange, Bogi Hansen, and Hedinn Valdimarsson. Influence of the Atlantic Subpolar Gyre in the Thermohaline Circulation. *Science*, 309(5742):1841–1844, 2005.

[33] D. S. Dukhovskoy, I. Yashayaev, A. Proshutinsky, J. L. Bamber, I. L. Bashmachnikov, E. P. Chassignet, C. M. Lee, and A. J. Tedstone. Role of Greenland Freshwater Anomaly in the Recent Freshening of the Subpolar North Atlantic. *Journal of Geophysical Research. Oceans*, 124(5):3333–3360, 2019.

[34] N. Penny Holliday, Manfred Bersch, Barbara Berx, Leon Chafik, Stuart Cunningham, Hjálmar Hátún, William Johns, Simon A. Josey, Karin Margretha H. Larsen, Sandrine Mulet, Marilena Oltmanns, Gilles Reverdin, Tom Rossby, Virginie Thierry, Hedinn Valdimarsson, and Igor Yashayaev. Wind-driven ocean Circulation changes cause the largest freshening event for 120 years in subpolar North Atlantic. *Nature Communications*, 11(585):1–15, 2020.

[35] John Marshall and R. Alan Plumb. *Atmosphere, Ocean, and Climate Dynamics: An Introductory Text*. Elsevier Academic Press, 2008.

[36] Matthias Tomczak and J. Stuart Godfrey. *Regional Oceanography: An Introduction*. Pergamon, 1994.

[37] A. Birol Kara, Peter A. Rochford, and Harley E. Hurlburt. Mixed layer depth variability over the global ocean. *Journal of Geophysical Research*, 108(C3):24–1 – 24–15, 2003.

[38] K. Lorbacher, D. Dommenget, P. P. Niiler, and A. Köhl. Ocean mixed layer depth: A subsurface proxy of ocean-atmosphere variability. *Journal of Geophysical Research*, 111(C07010):1–22, 2006.

[39] Klaus Peter Koltermann, Viktor Gouretski, and Kai Jancke. WOCE Atlas Volume 3: Atlantic Ocean, 2011. `http://whp-atlas.ucsd.edu/atlantic/a16/sections/printatlas/printatlas.htm`, last accessed: October 2, 2019.

[40] Philip Sexton. The Deep: Polar 'pumps', 2017. `https://www.open.edu/openlearn/nature-environment/environmental-studies/the-deep-polar-pumps`, last accessed: October 2, 2019.

[41] Anand Gnanadesikan. A simple predictive model for the structure of the oceanic pycnocline. *Science*, 283(5410):2077–2079, 1999.

[42] Dan Seidov, Alexey Mishonov, James Reagan, and Rost Parsons. Eddy–Resolving In Situ Ocean Climatologies of Temperature and Salinity in the Northwest Atlantic Ocean. *Journal of Geophysical Research: Oceans*, 124(1):41–58, 2019.

[43] R. T. Sutton and M. R. Allen. Decadal Predictability of North Atlantic sea surface temperature and climate. *Nature*, 388:563–567, 1997.

[44] Matthew W. Schmidt, Maryline J. Vautravers, and Howard J. Spero. Rapid subtropical North Atlantic salinity oscillations across Dansgaard-Oeschger cycles. *Nature*, 443(7111):561–564, 2006.

[45] Damien Desbruyères. *The Meridional Overturning Circulation variability and heat content changes in the North Atlantic subpolar gyre*. PhD, Université de Bretagne Occidentale, Bretagne, 2013.

[46] John H. Steele, Karl K. Turekian, and S. A. Thorpe. *Encyclopedia of Ocean Sciences: Florida Current, Gulf Stream and Labrador Current*. Elsevier, Amsterdam, 2001.

[47] Friedrich A. Schott, Rainer Zantopp, Lothar Stramma, Marcus Dengler, Jürgen Fischer, and Mathieu Wibaux. Circulation and Deep-Water Export at the Western Exit of the Subpolar North Atlantic. *Journal of Physical Oceanography*, 34:817–843, 2004.

[48] Alice Marzocchi, Joël J.-M. Hirschi, N. Penny Holliday, Stuart A. Cunningham, Adam T. Blaker, and Andrew C. Coward. The North Atlantic subpolar circulation in an eddy-resolving global ocean model. *Journal of Marine Systems*, 142:126–143, 2015.

[49] David J. R. Thornalley, Delia W. Oppo, Pablo Ortega, Jon I. Robson, Chris M. Brierley, Renee Davis, Ian R. Hall, Paola Moffa-Sanchez, Neil L. Rose, Peter T. Spooner, Igor Yashayaev, and Lloyd D. Keigwin. Anomalously weak Labrador Sea

convection and Atlantic overturning during the past 150 years. *Nature*, 556:227–242, 2018.

[50] L. Caesar, S. Rahmstorf, A. Robinson, G. Feulner, and V. Saba. Observed fingerprint of a weakening Atlantic Ocean overturning circulation. *Nature*, 556(7700):191–196, 2018.

[51] Summer K. Praetorius. North Atlantic circulation slows down, 2018. `https://www.nature.com/articles/d41586-018-04086-4/`, last accessed: October 2, 2019.

[52] Léon Chafik and T. Rossby. Volume, Heat, and Freshwater Divergences in the Subpolar North Atlantic Suggest the Nordic Seas as Key to the State of the Meridional Overturning Circulation. *Geophysical Research Letters*, 46(9):4799–4808, 2019.

[53] M.-A. Sicre, K. Weckström, M.-S. Seidenkrantz, A. Kuijpers, M. Benetti, G. Masse, U. Ezat, S. Schmidt, I. Bouloubassi, J. Olsen, M. Khodri, and J. Mignot. Labrador current variability over the last 2000 years. *Earth and Planetary Science Letters*, 400:26–32, 2014.

[54] John A. Church. A Change in Circulation? *Science*, 317(5840):907–909, 2007.

[55] Martha W. Buckley and John Marshall. Observations, inferences, and mechanisms of the Atlantic Meridional Overturning Circulation: A review. *Reviews of Geophysics*, 54(1):5–63, 2016.

[56] John Marshall, Alistair Adcroft, Chris Hill, Lev Perelman, and Curt Heisey. A finite-volume, incompressible Navier Stokes model for studies of the ocean on parallel computers. *Journal of Geophysical Research*, 102(C3):5753–5766, 1997.

[57] Alistair Adcroft, Chris Hill, Jean-Michel Campin, John Marshall, and Patrick Heimbach. Overview of the formulation and numerics of the MIT GCM, 2004.

[58] Alistair Adcroft, Jean-Michel Campin, Stephanie Dutkiewicz, Constantinos Evangelinos, David Ferreira, Gael Forget, Baylor Fox-Kemper, Patrick Heimbach, Chris Hill, Ed Hill, Helen Hill, Oliver Jahn, Martin Losch, John Marshall, Guillaume Maze, Dimitris Menemenlis, and Andrea Molod. MITgcm User Manual, 2018.

[59] Ou Wang, Ichiro Fukumori, and Ian Fenty. An Overview of ECCO Version 4 Release 3's ftp Site. *Jet Propulsion Laboratory*, 2017.

[60] Christopher G. Piecuch. A Note on Practical Evaluation of Budgets in ECCO Version 4 Release 3. *Jet Propulsion Laboratory*, 2017.

[61] Argo. Argo float data and metadata from Global Data Assembly Centre (Argo GDAC), 2020. `https://doi.org/10.17882/42182`.

[62] SEaOS. Southern Elephant seals as Oceanographic Samplers, 2009. `http://biology.st-andrews.ac.uk/seaos/`.

[63] Timothy P. Boyer, John I. Antonov, Olga K. Baranova, Hernan E. Garcia, Daphne R. Johnson, Alexey V. Mishonov, Todd D. O'Brien, Dan Seidov, I. Smolyar, Melissa M. Zweng, Christopher R. Paver, Ricardo A. Locarnini, James R. Reagan, Carla Coleman, and Alexandra Grodsky. World ocean database 2013, 2013.

[64] Ian Fenty, Ichiro Fukumori, and Ou Wang. ECCO | Latest Product, 2020. `https://ecco.jpl.nasa.gov/products/latest/`, last accessed: January 15, 2020.

[65] Python Tutorial. Plotting Tiles — ECCO Version 4 Python Tutorial 1.0 documentation, 2019. `https://ecco-v4-python-tutorial.readthedocs.io/ECCO_v4_Plotting_Tiles.html`, last accessed on May 21, 2019.

[66] MATLAB. *9.1.0.441655 (R2016b)*. The MathWorks Inc., Natick, Massachusetts, 2016.

[67] Paul Barker. Thermodynamic Equation of SeaWater TEOS-10, 2011. `http://www.teos-10.org/software.htm`, last accessed: January 6, 2020.

[68] David Pugh. *Changing Sea Levels: Effects of Tides, Weather and Climate*. Cambridge University Press, Cambridge, 2004.

[69] Georgy L. Shevlyakov and Hannu Oja. *Robust correlation: Theory and applications*. Wiley series in probability and statistics. Wiley, Chichester West Sussex, 2016.

[70] Christian-Diedrich Schönwiese. *Praktische Statistik für Meteorologen und Geowissenschaftler*. Gebrürder Borntraeger, Berlin, 4th edition, 2006.

[71] Calvin Dytham. *Choosing and Using Statistics: A Biologist's Guide*. Wiley-Blackwell, 3rd edition, 2011.

[72] Curtis D. Mobley, editor. *Developments in Atmospheric Science: Principal Component Analysis in Meteorology and Oceanography*, volume 17. Elsevier, Amsterdam, 1988.

[73] Steven Herbette. Empirical Orthogonal Functions (PCA) Principal Components Analysis (EOF), 2019. `https://www.google.com/url?sa=t&rct=j&q=&esrc=s&source=web&cd=3&cad=rja&uact=8&ved=2ahUKEwjG9PPjtJ7lAhUDMewKHVaqA6AQFjACegQIAxAC&url=http%3A%2F%2Fstockage.univ-brest.fr%2F~herbette%2FData-Analysis%2Fdata_analysis_eof.pdf&usg=AOvVaw1QJROt42cycJ3ujYMYMpc_`.

[74] Sirpa Häkkinen and Peter B. Rhines. Decline of subpolar North Atlantic circulation during the 1990s. *Science*, 304(5670):555–559, 2004.

[75] Nicolas P. Foukal and M. Susan Lozier. Assessing variability in the size and strength of the North Atlantic subpolar gyre. *Journal of Geophysical Research*, 122:6295–6308, 2017.

[76] A. M. Treguier, S. Theetten, E. P. Chassignet, T. Penduff, R. Smith, L. Talley, J. O. Beismann, and C. Böning. The North Atlantic Subpolar Gyre in Four High-Resolution Models. *American Meteorological Society*, 35:757–774, 2005.

[77] Christophe Herbaut and Marie-Noëlle Houssais. Response of the eastern North Atlantic subpolar gyre to the North Atlantic Oscillation. *Geophysical Research Letters*, 36(17):223, 2009.

[78] A. Born, T. F. Stocker, and A. B. Sandø. Coupling of eastern and western subpolar North Atlantic: salt transport in the Irminger Current. *Ocean Science Discussions*, 10(2):555–579, 2013.

[79] Zeliang Wang, David Brickman, Blair J. W. Greenan, and Igor Yashayaev. An abrupt shift in the Labrador Current System in relation to winter NAO events. *Journal of Geophysical Research: Oceans*, 121(7):5338–5349, 2016.

[80] Kjetil Våge, Robert S. Pickart, Virginie Thierry, Gilles Reverdin, Craig M. Lee, Brian Petrie, Tom A. Agnew, Amy Wong, and Mads H. Ribergaard. Surprising return of deep convection to the subpolar North Atlantic Ocean in winter 2007–2008. *Nature Geoscience*, 2(1):67–72, 2009.

[81] A. Piron, V. Thierry, H. Mercier, and G. Caniaux. Gyre–scale deep convection in the subpolar North Atlantic Ocean during winter 2014–2015. *Geophysical Research Letters*, 44(3):1439–1447, 2017.

[82] Marieke Femke de Jong and Laura de Steur. Strong winter cooling over the Irminger Sea in winter 2014-2015, exceptional deep convection, and the emergence of anomalously low SST. *Geophysical Research Letters*, 43(13):7106–7113, 2016.

[83] Patricia Handmann. *Deep Water Formation and Spreading Dynamics in the subpolar North Atlantic from Observations and high-resolution Ocean Models*. Dissertation, Christian-Albrechts-Universität zu Kiel, Kiel, 2019.

[84] Amy S. Bower and Heather D. Hunt. Lagrangian Observations of the Deep Western Boundary Current in the North Atlantic Ocean. Part I: Large-Scale Pathways and Spreading Rates. *Journal of Physical Oceanography*, 30:764–783, 2000.

[85] Jan Klaus Rieck. *The Nature and Variability of Eddy Kinetic Energy in an Ocean General Circulation Model: With a Focus on the South Pacific Subtropical Gyre and the Labrador Sea*. Dissertation, Christian-Albrechts-Universität zu Kiel, Kiel, 2019.

[86] Jonathan Gula, Tanya M. Blacic, and Robert E. Todd. Submesoscale Coherent Vortices in the Gulf Stream. *Geophysical Research Letters*, 46(5):2704–2714, 2019.

[87] Dujuan Kang and Enrique N. Curchitser. Gulf Stream eddy characteristics in a high-resolution ocean model. *Journal of Geophysical Research: Oceans*, 118(9): 4474–4487, 2013.

[88] Kara L. Lavender, Russ E. Davis, and W. Brechner Owens. Mid-depth recirculation observed in the interior Labrador and Irminger seas by direct velocity measurements. *Nature*, 407:66–69, 2000.

[89] R. H. Käse, A. Biastoch, and D. B. Stammer. On the mid-depth circulation in the Labrador and Irminger Seas. *Geophysical Research Letters*, 28(18):3433–3436, 2001.

[90] Fiammetta Straneo, Robert S. Pickart, and Kara Lavender. Spreading of Labrador sea water: an advective-diffusive study based on Lagrangian data. *Deep Sea Research Part I: Oceanographic Research Papers*, 50(6):701–719, 2003.

[91] Thomas L. Delworth and Richard J. Greatbatch. Multidecadal Thermohaline Circulation Variability Driven by Atmospheric Surface Flux Forcing. *Journal of Climate*, 13:1481–1495, 2000.

[92] Axel Schweiger, Ron Lindsay, Jinlun Zhang, Mike Steele, Harry Stern, and Ron Kwok. Uncertainty in modeled Arctic sea ice volume. *Journal of Geophysical Research*, 116(24):L16501, 2011.

Acknowledgements

At this point, I like to give my acknowledgements in the first place to Dr. Marilena Oltmanns, who supervised my work with helpful comments and impulses where to set focuses. She always had new ideas and showed different perspectives to solve problems and to understand the many interdependet mechanisms in the ocean basins and the atmosphere. With a lot of patience she introduced me to the basics of subpolar oceanography and gave me a lot of space to ask questions. I would also like to thank her for her support for participating in YOUMARES, where I got many helpfull and motivating impressions of and inputs from the oceanographic community.

Another person I want to give my thanks to is Dr. Johannes Karstensen. He established the contact to Dr. Oltmanns and therefore made it possible for me to come to the GEOMAR. Also, he gave me the opportunity to participate on a research cruise in the baltic sea. From this excursion I gained a lot of insights into the measurement methods of oceanographers.

Of course the GEOMAR itself must not remain unmentioned. The employees have given me access to the scientific facilities, versatile academic literature and evaluation software without complications. I was also provided with a workplace among experts in the field of oceanography. Also, I was able to broaden and deepen my understanding in the many different lectures and seminars offered by the institute for the local courses of study.

In addition, I can say that it was a great pleasure to work with my office colleagues. The conversations with them stimulated the discussion about the results and often quickly cleared up misunderstandings.

None of this would have been realizable without Prof. Dr. Jörg Enderlein who made it possible for me, as a student of the University of Göttingen, to write my thesis in Kiel.

Erklärung nach §12(9) der Prüfungsordnung für den Bachelor-Studiengang Physik und den Master-Studiengang Physik an der Universität Göttingen:

Hiermit erkläre ich, dass ich diese Abschlussarbeit selbständig verfasst habe, keine anderen als die angegebenen Quellen und Hilfsmittel benutzt habe und alle Stellen, die wörtlich oder sinngemäß aus veröffentlichten Schriften entnommen wurden, als solche kenntlich gemacht habe.
Darüberhinaus erkläre ich, dass diese Abschlussarbeit nicht, auch nicht auszugsweise, im Rahmen einer nichtbestandenen Prüfung an dieser oder einer anderen Hochschule eingereicht wurde.

Göttingen, den 25. Februar 2020

(Anna-Marie Strehl)